NAL PROPOSAL No. 203

Scientific Spokesman:

M. Strovink
Joseph Henry Laboratories
Princeton University
Princeton, New Jersey 08540

FTS/Off-net: 609-599-3511
452-4369

Feasible Search for Heavy Neutral Muons Predicted by Gauge Theories

R. Cester, C. M. Hoffman, F. C. Shoemaker, and M. Strovink

Joseph Henry Laboratories
Princeton University

Princeton, New Jersey 08540

March 9, 1973

ABSTRACT

Predictions of gauge theories, which hold forth the tantalizing prospect of a unified, renormalizable picture of weak and electromagnetic interactions, must be comprehensively tested. Neutral heavy leptons, present in most gauge theories, are prime candidates for search. New information about them is expected from no existing or planned experiment anywhere. We propose here a definitive search for neutral heavy muons in the mass range 2-10 GeV.

The apparatus, consisting mainly of magnetized iron slabs and proportional chambers, is to occupy the downstream portion of the NAL Muon Laboratory. The experiment requires 10^{12} 200 GeV muons, which may concurrently illuminate the Muon Scattering Facility target upstream. Strong features of the proposed spectrometer make possible additional new measurements.

CONTENTS

I. INTRODUCTION

A. Predictions of Gauge Theories

The recently-developed spontaneously-broken gauge theories of weak interactions[1] have by now generated intense interest, and widespread theoretical and experimental activity. The idea of spontaneously broken gauge symmetry leads to unified theories of electromagnetic and weak interactions, which avoid the high-energy divergence of the Fermi theory. If supported by experiment, gauge theories represent the most important advance in understanding of weak interactions since the V-A hypothesis was put forth more than fifteen years ago.

So far, most of the pertinent experimental effort has focussed on neutral currents which couple to neutrinos, as predicted by the original Weinberg model.[2] The experimental situation at the time of the NAL-Chicago Conference is summarized by Perkins.[3] Taken at face value, the $\bar{\nu}_e e^- \to e^- \bar{\nu}_e$ and $\nu N \to \nu N \pi^o$ experiments together rule out that model. Difficulties in executing and interpreting these experiments appear to mitigate that conclusion, although in any case the possible range of the Weinberg model's parameter has been severely restricted. A definitive test awaits the completion this year of the CERN-Gargamelle $\overset{(-)}{\nu}_\mu e^- \to \overset{(-)}{\nu}_\mu e^-$ exposure.

In general, gauge theories avoid divergent amplitudes by introducing cancelling diagrams, involving neutral currents, or heavy leptons, or both. Without neutral currents, one must have heavy leptons. Some divergent diagrams involve exchange of a neutrino. To cancel these amplitudes without neutral currents, one must have <u>neutral</u> heavy leptons. Bjorken and Llewellyn Smith[4] have catalogued the varieties of neutral currents and heavy leptons, and their couplings, found in six simple gauge theories. Table 1 contains the subset of that information which is most pertinent to this discussion.

Table 1

Theory	I (Weinberg[2])	II (Lee, Prentki, Zumino (Ref. 5))	III	IV	V	VI (Georgi, Glashow (Ref. 6))
Leptons interacting via (V-A) current	2	3	2	3	2	3
Leptons interacting via (V+A) current	1	1	2	2	3	3
Heavy charged muon (has nonzero coupling to μ-neutrino)	-	M^+	-	M^+	-	M^+
Heavy neutral muon (has nonzero (V+A) coupling)	-	-	M^o	x^o	M^o	M^o
$\frac{\sigma(\mu^+(L.H.)N \to \bar{M}^o X)}{\sigma(\nu N \to \mu^- X)}$ $(s \gg M^2_{M^o})$	-	-	1	$\frac{1}{2\cos^2\alpha}$	2	$\frac{1}{\sin^2\alpha}$ (a)
$\frac{M^o \text{mass}}{M^+ \text{mass}}$	-	-	-	?	$\frac{1}{\sqrt{2}}$ (b)	$\frac{1}{2\lvert\sin\alpha\rvert}$
$\frac{\Gamma(\bar{M}^o \xrightarrow{V-A} \mu^+ X)}{\Gamma(\bar{M}^o \xrightarrow{V+A} \mu^+ X)}$	-	-	0	0	$\gtrsim 0$	$\cos^2\alpha$

(a) In Theory VI, $|\sin\alpha| = M_W/(53\ \text{GeV})$.

(b) Here we refer to an M^+ which does not couple to μ-neutrinos.

Of the five simplest theories which contain heavy leptons, four contain neutral heavy leptons with (V + A) coupling. Three theories contain charged heavy leptons which couple to conventional neutrinos. An even larger fraction of more complicated gauge theories, with more heavy leptons, make provision for neutral heavy leptons.

Experiments searching for heavy leptons or weak bosons predicted by gauge theories can yield mainly positive information. That is to say, with few exceptions,[7] existing experimental and theoretical information cannot guarantee that the weakon and lepton masses lie in an experimentally accessible range. One simply hopes that available beam energies are adequate. In this optimistic framework, search for a neutral heavy lepton, having nonzero V + A coupling, has a special appeal. While "equally" likely to exist from the gauge-theoretical viewpoint, such particles do not arise from simple-minded extrapolations of the e^-, ν_e ; μ^-, ν_μ sequence. Discovery of massive neutral leptons would be compelling evidence in support of spontaneously-broken gauge theories.

B. General Experimental Considerations

Neutral heavy leptons can be created only through weak production or decay. Mass limits $\gtrsim$ 0.5 GeV are imposed by the unobserved decays $K^+ \to e^+ E^\circ$, $K^+ \to \mu^+ M^\circ$. No existing or already-proposed experiment, at any laboratory, can improve these limits. A corresponding lower bound of 0.9 GeV (95% conf.) on the mass of the short-lived charged heavy lepton, obtained at Frascati, was reported by Zichichi at the NAL-Chicago Conference.

Since cross-sections of electromagnetic background processes are much smaller for muons than for electrons, we concentrate here on the reaction

$$\text{(left-handed)}\ \mu^+ N \to \bar{M}^o X\ ; \qquad (1)$$
$$\bar{M}^o \to \mu^+ \mu^- \bar{\nu}_\mu$$
$$\to \mu^+ e^- \bar{\nu}_e$$
$$\to \mu^+ + \text{hadrons}\ .$$

With mass exceeding 1 GeV, the M^o has a short lifetime ($< 10^{-11}$ sec), and is revealed only through its decay products. The $\mu^+ \mu^- \bar{\nu}_\mu$ final state has a clear signature of apparent muon nonconservation. Bjorken and Llewellyn Smith[4] have estimated the hadronic branching ratio to be 50%; in later calculations, we take the $\mu^+ \mu^- \bar{\nu}_\mu$ branching ratio to be 25%. The $\mu^+ e^- \bar{\nu}_e$ final state is scarcely distinguishable from $\mu^+ - e^-$ scattering, and the hadronic final state from $\mu^+ - N$ scattering.

A μ^+ beam obtained from forward π^+ decay has largely left-handed polarization. This is a traditional objection to studying muon-induced weak interactions at proton synchrotrons. However, the theories enumerated in Table 1 which contain the $\bar{M}^o$, predict it to have a weak V + A coupling at least equal to, and often much larger than its V - A coupling. In the $s \gg M^2_{M^o}$ limit, Table 1 shows that the cross-section for reaction (1) is of the order of, or greater than, the total $\nu - N$ cross-section.

The importance of searching for heavy neutral leptons rests on the fact that they are new and different hypothetical particles. If they exist, charged and neutral heavy leptons differ in mass, and in modes of production and decay. For example, in the Georgi-Glashow theory (VI), with $M_W = 37$ GeV, Primack and Quinn[7] have found that muon-anomalous-magnetic-moment measurement sets an <u>upper</u> limit $M_{M^+} \lesssim 6$ GeV. For the same conditions, the neutral heavy muon is lighter ($M_{M^o} \lesssim 4$ GeV), and is produced with twice the $\nu - N$ total cross-section in the high-energy limit.

Except for the argument that searching for heavy neutral leptons is of independent interest, one might think that assumed experimental advantages make it sufficient, initially, to search only for charged heavy leptons. But

these assumed experimental advantages do not exist. The following is a brief general comparison between muoproducing an M^o, and photoproducing an $M^+ M^-$ pair, as in NAL Experiment #87[8].

1. Kinematic limit on heavy lepton mass. The muon produces only one heavy lepton, while the photon must create two. One needs a 1600 GeV accelerator to achieve the same absolute limit on photoproduced M^+ or M^- mass, as can be reached with 400 GeV protons using M^o muoproduction.

2. Production cross-section. Charged heavy leptons are produced electromagnetically, whereas neutral heavy leptons are produced weakly. However, the photoproduction diagram is suppressed by a (lepton mass)$^{-4}$ factor. In addition, attenuation in photon beam energy limits the target thickness to ~ 0.5 radiation lengths. A 200 GeV muon, on the other hand, loses only 1/8 of its energy in passing through 30 ft of steel. (In Part II we introduce a muon spectrometer with this target thickness.) Multiplying the production cross-section by the number of target particles per cm^2 gives the probability, per beam particle, for heavy lepton production. We have used the photoproduction cross-sections calculated for Be by Kim and Tsai[9], along with a muoproduction calculation of our own which gives essentially the same result as that of Ref. 4. (This calculation is described in Appendix A.) The results are shown as a function of heavy lepton mass in Fig. 1. The muoproduction probability lies above the photoproduction probability for masses exceeding 1.4 GeV. At 4 GeV heavy lepton mass, the muoproduction probability is greater by two orders of magnitude; at 8 GeV mass, by more than four orders of magnitude.

3. Available beam intensity. It is too early to compare the intensity

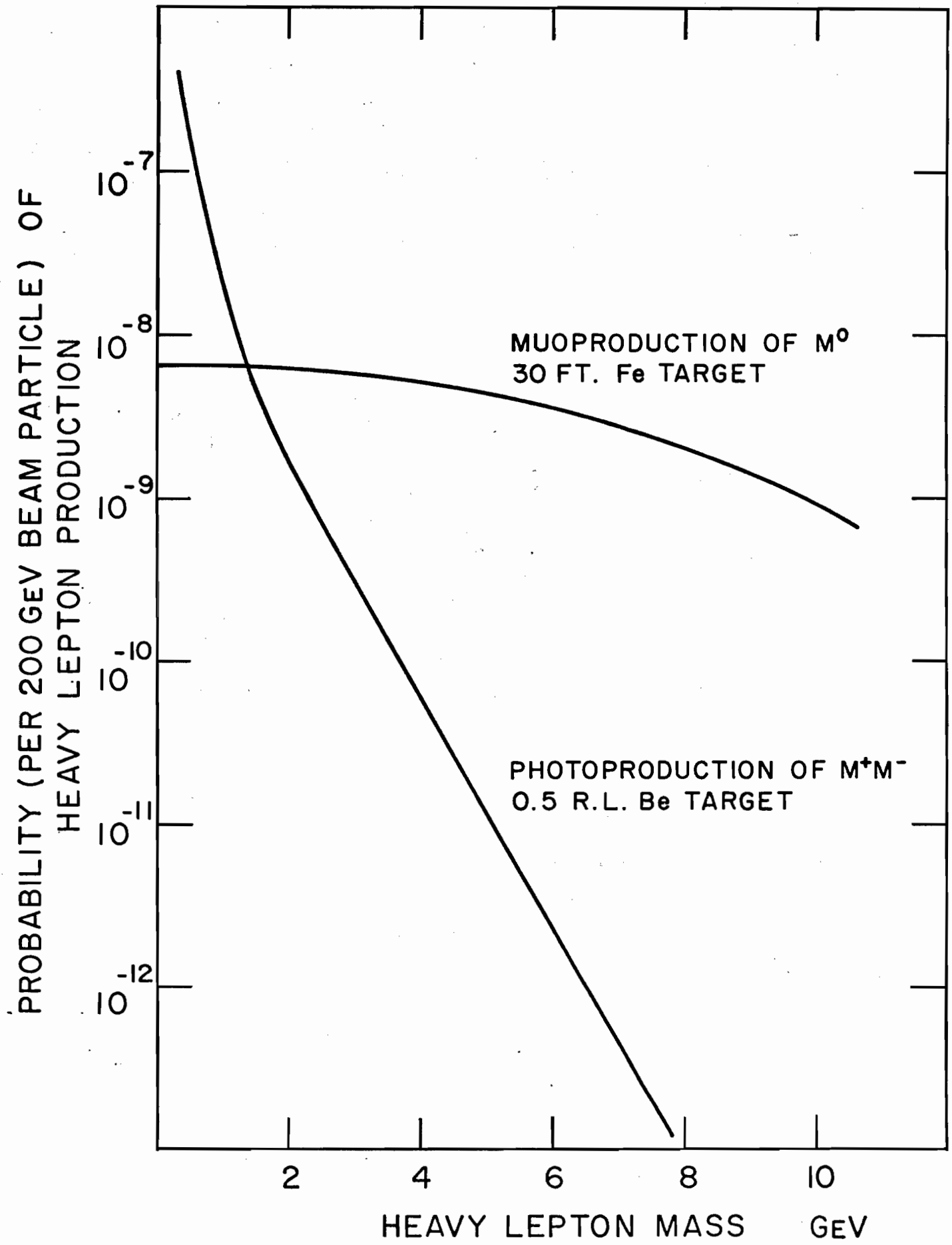
PROBABILITY (PER 200 GeV BEAM PARTICLE) OF HEAVY LEPTON PRODUCTION
10^{-7}
10^{-8}
10^{-9}
10^{-10}
10^{-11}
10^{-12}
MUOPRODUCTION OF M^0
30 FT. Fe TARGET
PHOTOPRODUCTION OF M^+M^-
0.5 R.L. Be TARGET
2
4
6
8
10
HEAVY LEPTON MASS GeV

Figure 1

of the NAL photon beam, which has not been tested, to that of the NAL muon beam, which is being designed. It will be shown below that a total of 10^{12} 200 GeV muons is needed for the heavy neutral muon search. This is 60% of the integrated flux recently envisaged by Experiment 98 [10]. The same 200 GeV muons could be used by both experiments. We argue in Appendix C that delivery of 10^{12} muons to an experiment represents a practical and reasonable NAL goal.

4. Recognition of the heavy lepton. The photoproduction experiment makes use of the decay modes

$$M^+ \to \nu_\mu \, \nu_e \, e^+ \ (\sim 20\%) \text{ or } \nu_\mu \, \nu_\mu \, \mu^+ \ (\sim 40\%) \ ;$$
$$M^- \to \bar{\nu}_\mu \, \bar{\nu}_\mu \, \mu^- \ (\sim 40\%) \text{ or } \bar{\nu}_\mu \, \bar{\nu}_e \, e^- \ (\sim 20\%) \ .$$

(Ref. 4 estimates the $\nu\,\pi$ branching ratio to be negligible for heavy lepton masses above 3 GeV.) Also, both charged leptons are required to appear on the same side of the beam. The full coincidence occurs less than $\sim 10\%$ of the time. The use of these modes requires the M^+ (M^-) to couple to ν_μ ($\bar{\nu}_\mu$), making the experiment insensitive to heavy leptons with only right-handed coupling, as in Theory V (see Table 1). On the other hand, in the muoproduction experiment the decay $\bar{M}^o \to \mu^+ \, \mu^- \, \bar{\nu}_\mu$ has a branching ratio of $\sim 25\%$. Of the seven particles in the initial and final state of the photoproduction experiment, five are unseen neutrals. Of the four leptons in the muoproduction experiment, only one is unseen.

Charged heavy muons also can be produced at NAL by the reaction[11]

$$\nu_\mu \, N \to M^+ \, X \ ; \ M^+ \to \nu_\mu \, \nu_\mu \, \mu^+ \text{ or } \nu_\mu \, X \ .$$

The experiment is analagous to the one put forth here, except that the momentum of at most one charged particle can be measured.

II. EXPERIMENTAL PLAN

We plan to search for neutral heavy muons, using the production and decay modes

$$\text{(left-handed)}\ \mu^+ N \to \bar{M}^o X;$$

$$\bar{M}^o \to \mu^+ \mu^- \bar{\nu}_\mu\ (\sim 25\%).$$

The production cross-section, multiplied by the number of nucleons/cm^2 in a 30-ft Fe target, is shown as a function of M^o mass in Fig. 1.

A. High-Luminosity Muon Spectrometer

The experiment is intended to occupy the north portion of the Muon Laboratory, downstream of the Muon Scattering Facility[10] (Fig. 2). It is designed to make use of the same 200 GeV muons which impinge on that experiment's target.

The main elements of the muon spectrometer are 25 slabs of magnetized iron, and 26 multiwire proportional chambers (Fig. 3). The apparatus has the following special features:

1. A massive target consists of the 15 iron slabs which comprise the upstream 60% of the spectrometer; each slab is 2 ft thick. This is about one order of magnitude more nucleons/cm^2 than is usable in muon experiments without a distributed target. At 10^7 muons/4 sec, for example, the effective luminosity of the experiment is 10^{32}/cm^2-sec -- equal to the design figure for SPEAR or PEP. A 200 GeV muon loses an average of 12% of its energy in this target, which is 2% of a muon radiation length.
2. Fine-grained measurement of the muon trajectory is made by multi-

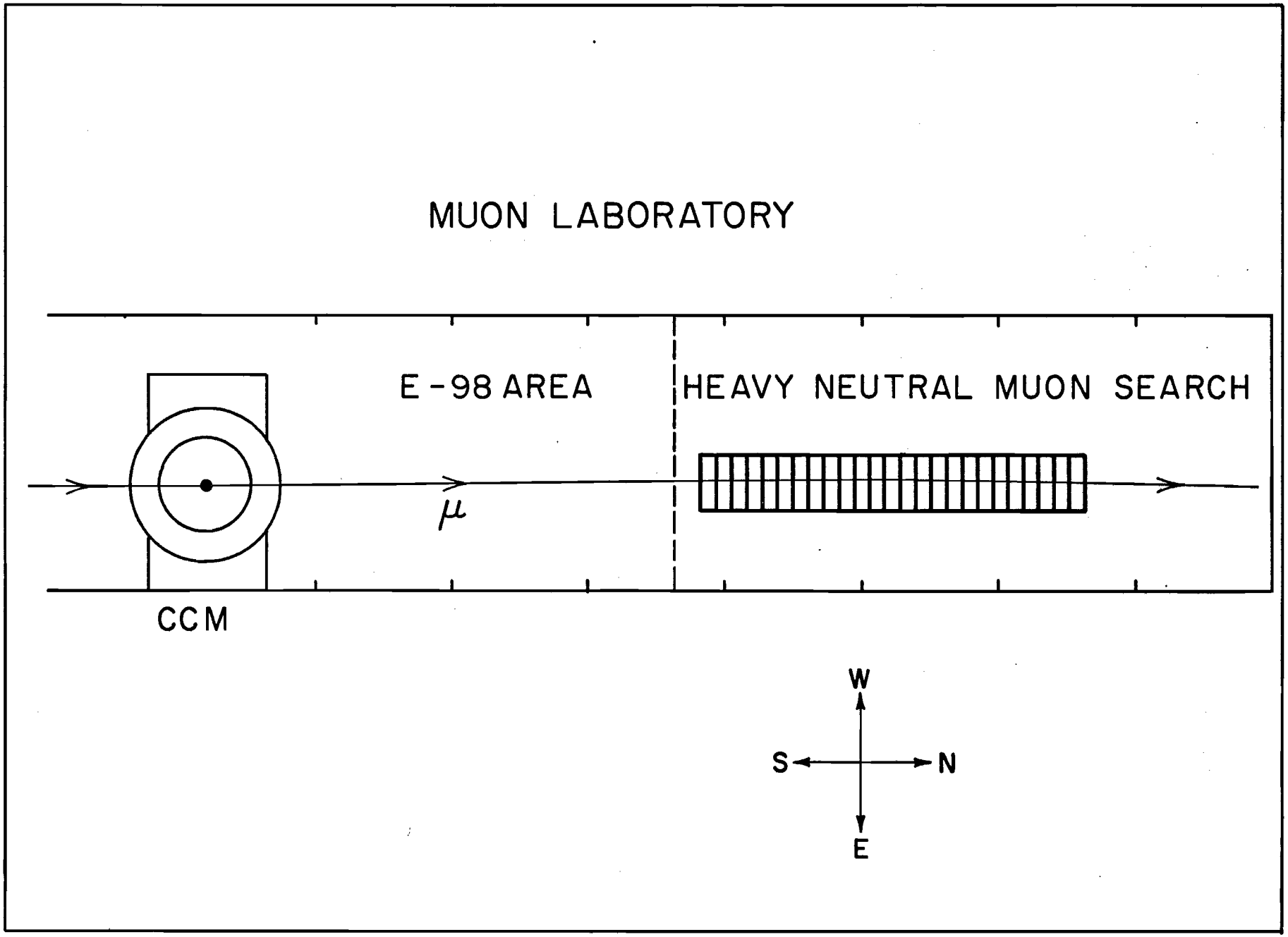
MUON LABORATORY
E-98 AREA
HEAVY NEUTRAL MUON SEARCH
μ
CCM
W
S
N
E

Figure 2

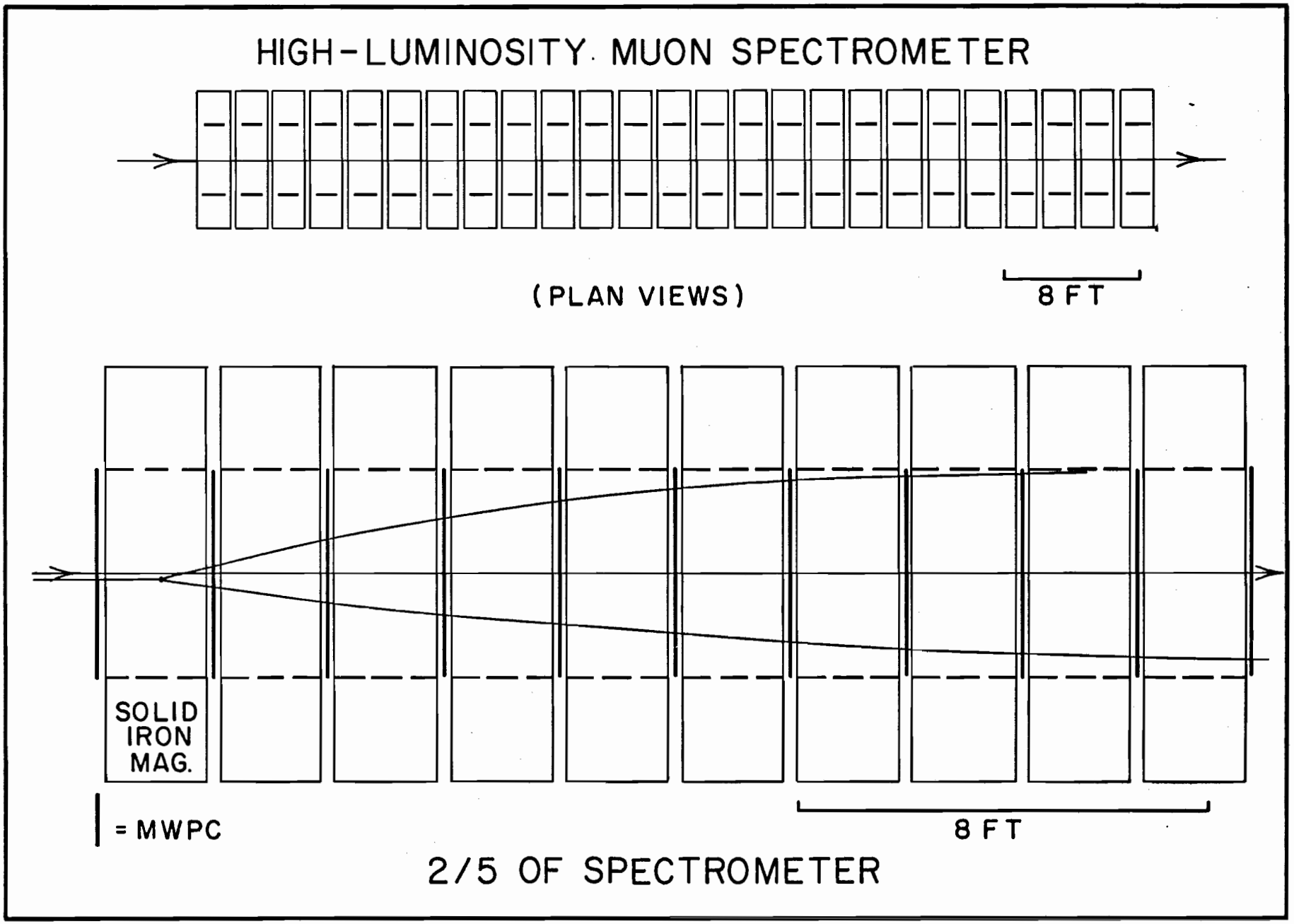
HIGH-LUMINOSITY MUON SPECTROMETER
(PLAN VIEWS)
8 FT
SOLID IRON MAG.
= MWPC
8 FT
2/5 OF SPECTROMETER

Figure 3

wire proportional chambers distributed every 27 in within the target. Dispersion of the final-state muon transverse momenta is thereby due to multiple Coulomb scattering occurring only in a small fraction of the target thickness. The proportional chambers will tolerate beam and halo intensities up to 10 MHz. Beam muons of known energy will be used as a continuous monitor of the momentum reconstruction.

3. The uniform cross-section of the spectrometer consists of the inner 3 x 4 ft portion of the iron slabs, magnetized vertically to 18.5 kG (Fig. 4). The field pattern is that of an ordinary filament-transformer core. This uniformity gives three benefits. First, no minimum production angle is required of the final-state muons, thereby enhancing the acceptance. Second, since both beam and halo pass through the chambers, there is no stringent requirement on the halo/beam ratio. Finally, there is no hole through which the beam is required to pass. Consequently, the experiment can operate even when the beam is focussed on the Muon Scattering Facility target, and deflected by the Chicago Cyclotron magnet. The latter effect makes it necessary to offset the muon spectrometer by ~ 2 ft with respect to the nominal beam line. If the cyclotron magnet is off, the dipoles in Enclosure 104 can be trimmed to achieve the same offset. The transverse momentum (8 GeV) of the magnetized iron slabs can be used to bend the muon beam into the berm downstream; or, if preferable, the spectrometer can be rotated 90° and the beam pitched into the ground.

4. A continuous iron medium is present, in which the event must develop.

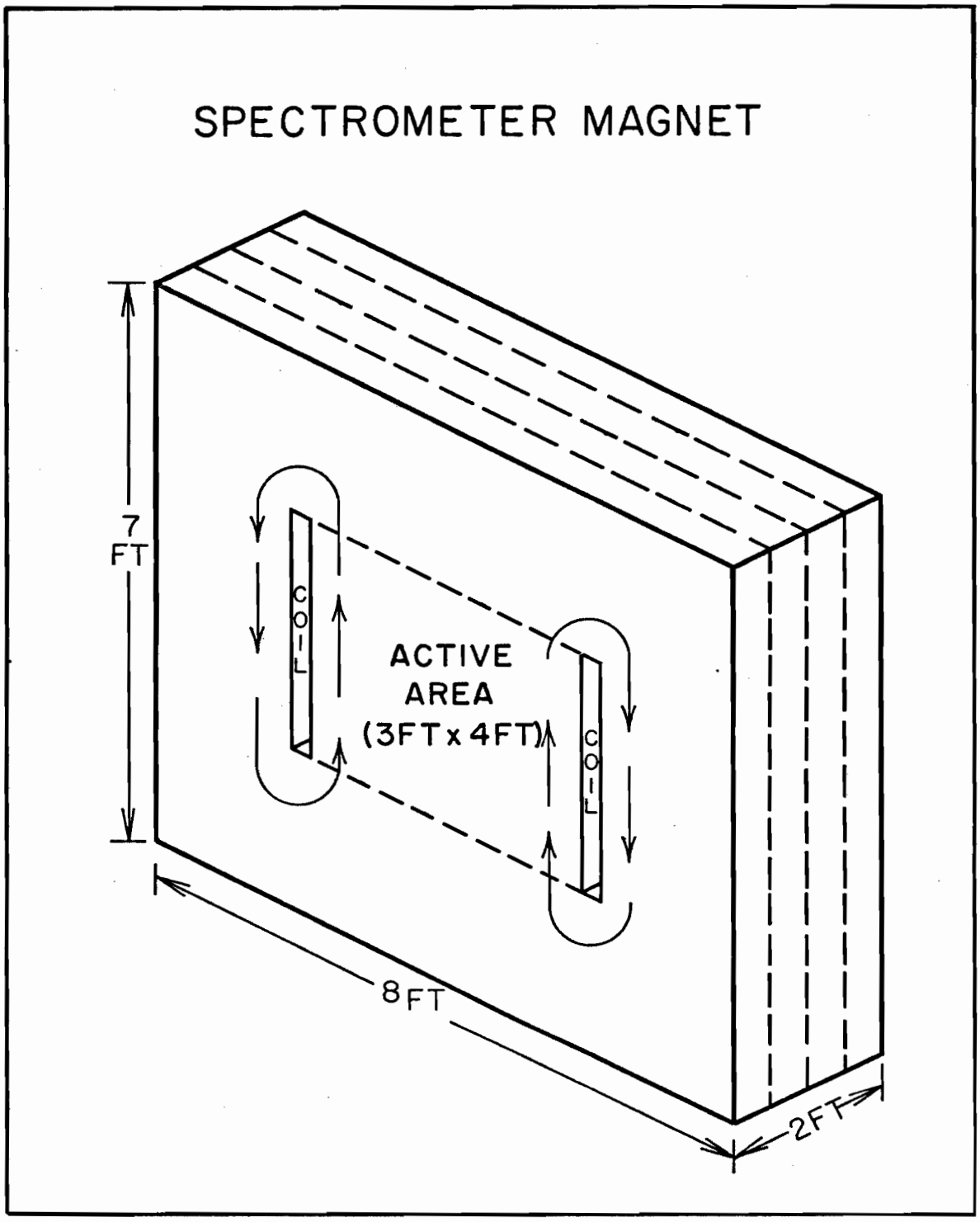
SPECTROMETER MAGNET
7 FT
COIL
ACTIVE AREA (3FT x 4FT)
COIL
8 FT
2FT

Figure 4

Muon identification is thereby simple. Pions are maximally constrained to interact before decaying into muons. The latter feature is crucial to suppression of background, as seen below.

An event trigger will be formed by requiring (1) evidence of muon energy transfer to particles which shower, and (2) appearance within the spectrometer of an additional muon. The energy transfer is measured by pulse-height analysis in (42) 1.5 ft x 1.5 ft scintillation counters distributed every 1 ft through the upstream 4/5 of the spectrometer and centered on the beam. A crack (not crossed by field lines!) will be left in each 2-ft-thick magnet to accomodate the odd counters. For an energy transfer of 80 GeV (typical for M_{M^o} = 4 GeV), there will be an average of ~ 120 hadron-shower-particle traversals of the four counters just downstream of the vertex. We plan to set a threshold of ~ 20 traversals. In addition, the pulse heights will be recorded for off-line analysis. We estimate that fluctuations in energy transfer and in shower statistics will cause good events to be rejected by this pulse-height requirement at a level ranging from 7% at small M^o mass to 20% at highest mass.

Evidence for production of an additional muon will come from 8 "picket-fence" hodoscopes of ~ 5 counters each, distributed through the middle 3/5 of the spectrometer. Two counts will be required in the one of these hodoscopes which lies an average of 12 ft of Fe downstream of the vertex. The hodoscopes upstream of the vertex are required to register only one count. In addition, to prevent interference by showers from coincident muon bremsstrahlung, the shower scintillators near the hodoscope registering two muons will be required to have a pulse height corresponding to fewer than ~ 5 particles.

Using this configuration, we have estimated the trigger rates due to

(1) μ-N scattering with soft $\pi \rightarrow \mu$ decay, (2) μ-trident production with muon bremsstrahlung, and (3) double muon bremsstrahlung. Each has an effective cross-section less than 1 nb ($4 * 10^6$ triggers). A somewhat larger trigger rate will arise from accidentals, if maximum (10 MHz) beam intensity is used. To minimize this rate, an additional hodoscope upstream of the spectrometer must veto events having two muons incident within the 10-nsec coincidence width of the system. With a veto efficiency of 99%, we estimate the accidental trigger rate to be $\lesssim$ 150 Hz (75/0.5 sec pulse) with 10 MHz beam intensity. Altogether, the trigger rate should not exceed 125/pulse, and the total number of triggers should be less than $25 * 10^6$.

The use of proportional chambers, which can be interrogated at a rate much higher than the trigger rate, permits two major simplifications of the triggering scheme. First, after the phototube discriminator outputs are latched, all the logic can be performed by low-cost TTL. Second, as a safety factor or means of further reducing the data rate, the on-line computer can make additional cuts on events before they are put on tape.

To sum up, the same iron slabs are used in this apparatus as (i) target, (ii) "prompt" hadron absorber, (iii) muon identifier, (iv) shower medium, (v) analyzing magnet. Functions (iii) and (v) presently are used by NAL Experiment 26[12], and functions (i), (ii), (iii), and (iv) by Experiment 21.[13]

B. Simulated Spectrometer Performance

A full Monte-Carlo simulation of the experiment was performed. The procedure for simulating production and decay of the $\bar{M}^o$ is detailed in Appendix A. In the $s >> M^2_{M^o}$ limit, the differential cross-section for $\bar{M}^o$ production was taken to be that for $\nu_\mu N \rightarrow \mu^- X$ in a spin - 1/2 parton model. Since,

typically, a Q^2 of only 35 $(GeV/c)^2$ is transferred to the target nucleon, this parton model was used not far beyond the range in which it is known to agree with experiment. The principal effect of finite $\bar{M}^o$ mass was to restrict available phase space. In decaying, the $\bar{M}^o$ was assumed to couple to the μ^+ via a (V + A) current, in agreement with the theories described in Table 1. In the limit of negligible muon mass the resulting distribution in the μ^+ or μ^- energy and angle, for example, is the same as that of the e^- in polarized muon decay. In general, the feasibility of the experiment does not depend on these details.

After creation within an 8 by 10-in beam area, the muon pair was propagated through ten magnets of the apparatus in Fig. 3. Multiple and single Coulomb scattering in the iron dispersed the muon transverse momenta; μ - e scattering and muon bremsstrahlung caused energy-loss straggling. An event was rejected if either muon failed to pass inside the 3 x 4-ft aperture of the six magnets just downstream of the vertex; or if either muon energy was below 2 GeV at the end of the sixth magnet. We made the worst-case assumption that the hadron shower accompanying M^o production would obliterate the muon track in proportional chambers upstream of the second of these six magnets. Thereby, a minimum of five measurements was possible on the muon trajectory.

The simulated event was reconstructed using a fitting procedure which made optimal use of the proportional-chamber information. This procedure is fully described in Appendix B. Briefly, a simultaneous least-squares fit was made to the longitudinal vertex position; the projected momentum and both direction tangents of each muon; and both projections of the multiple Coulomb scattering angle of each muon, in each of ten magnets. Iterative correction was made for muon energy loss. Because the measuring error is dominated by Coulomb scattering, proportional-chamber wire spacing of 5 mm could be used

with only ~ 20% deterioration in resolution, compared to the ideal case.

Results of the Monte-Carlo study were:

1. The acceptance of the spectrometer is 50% ± 5% over the full range of heavy lepton mass, from 0.5 to 10 GeV. Inefficiency is about equally attributable to effects of soft-muon range and spectrometer aperture.
2. The resolution, for a typical heavy lepton mass of 4 GeV, is ± 10.5% on the individual muon momenta, and ± 160 MeV/c on the vertical and horizontal transverse momenta of each muon. A kinematic distribution most sensitive to spectrometer resolution is the invariant mass spectrum of the two muons. Figure 5 shows the theoretical and reconstructed spectra. The resolution clearly is more than adequate.

C. Cost of Spectrometer

The major spectrometer components are the magnetized iron slabs, the proportional chambers, and the proportional-chamber electronics. In each case a substantial effort is made to minimize cost.

Magnets. The magnets depicted in Fig. 4 should be less costly than other solid iron magnets which have recently been constructed. Such magnets for NAL experiments have cost ~ $100/ton. A conservative estimate for the total cost of the magnet is then $67K. Appendix E contains a discussion of construction techniques.

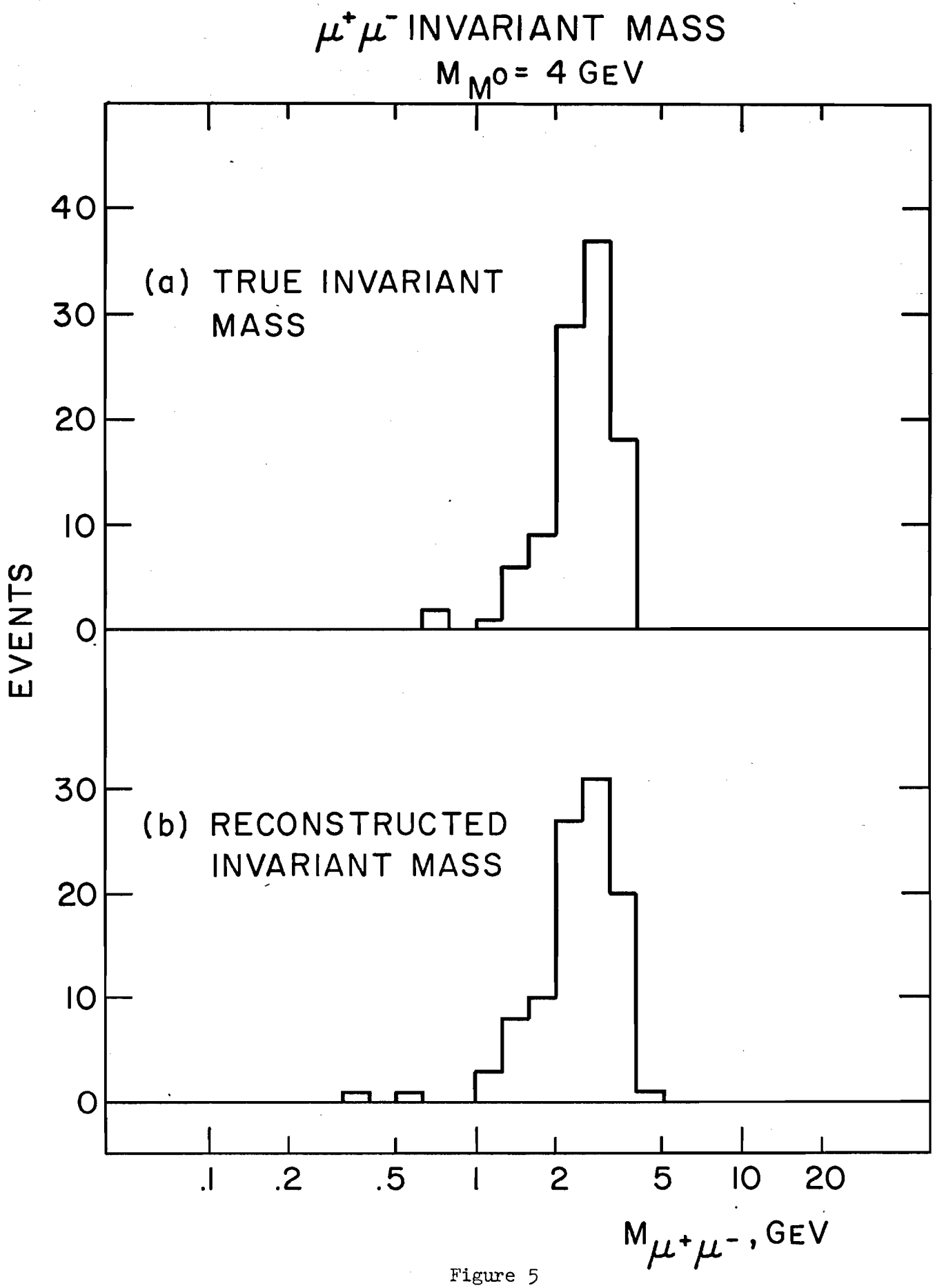
$\mu^+\mu^-$ INVARIANT MASS
M_{M^0} = 4 GeV
(a) TRUE INVARIANT MASS
(b) RECONSTRUCTED INVARIANT MASS
EVENTS
40
30
20
10
0
30
20
10
0
.1
.2
.5
1
2
5
10
20
$M_{\mu^+\mu^-}$, GeV

Figure 5

After the narrow slots are filled with iron, NAL can re-use the iron slabs to harden the passive muon shield, needed for higher-energy neutrino experiments. Alternatively, the magnets can be deployed as a more effective muon shield if used as a dispersive lens, similar to that designed by Kang et al.[14] The 8 GeV/c transverse momentum imparted to a 500 GeV muon displaces it 45 ft from the beam axis at the bubble chamber.

Proportional chambers. To improve proportional-chamber time resolution, it may be desirable to halve the wire spacing to 2.5 mm, reading out pairs of wires. We have built proportional chambers of similar wire spacing and span as early as three years ago.[15] Recently, the group constructing the External Muon Identifier[16] at NAL has used techniques which can reduce substantially the cost per plane. Printed strips on laminated outer planes sense the positive signals induced by avalanche at the inner wires, thereby tripling the number of planes per chamber. Figure 6 depicts proportional chambers of this type having the desired size. Tentatively, we estimate the cost (without electronics) as \$1K per chamber -- a total of \$26K.

Proportional-chamber electronics. To achieve $\lesssim$ 100 nsec time resolution with large track multiplicity, it will be necessary to use individual-wire electronics. At 5 mm wire spacing, a chamber of the type shown in Fig. 6 requires 720 electronics channels (for example, 15 48-channel circuit boards). An electronics system costing only \$2.50 per channel is being constructed for use at the Cornell electron synchrotron.[17] Also, we have prototyped a more compact circuit (Appendix D) which can be produced at comparable cost. At \$2.50 per channel, the total cost of proportional-chamber electronics will be \$47K.

To sum up, the main elements of the spectrometer require a capital investment of \$140K. Of this, \$67K is needed for iron re-usable by NAL, and \$73K for proportional chambers and electronics.

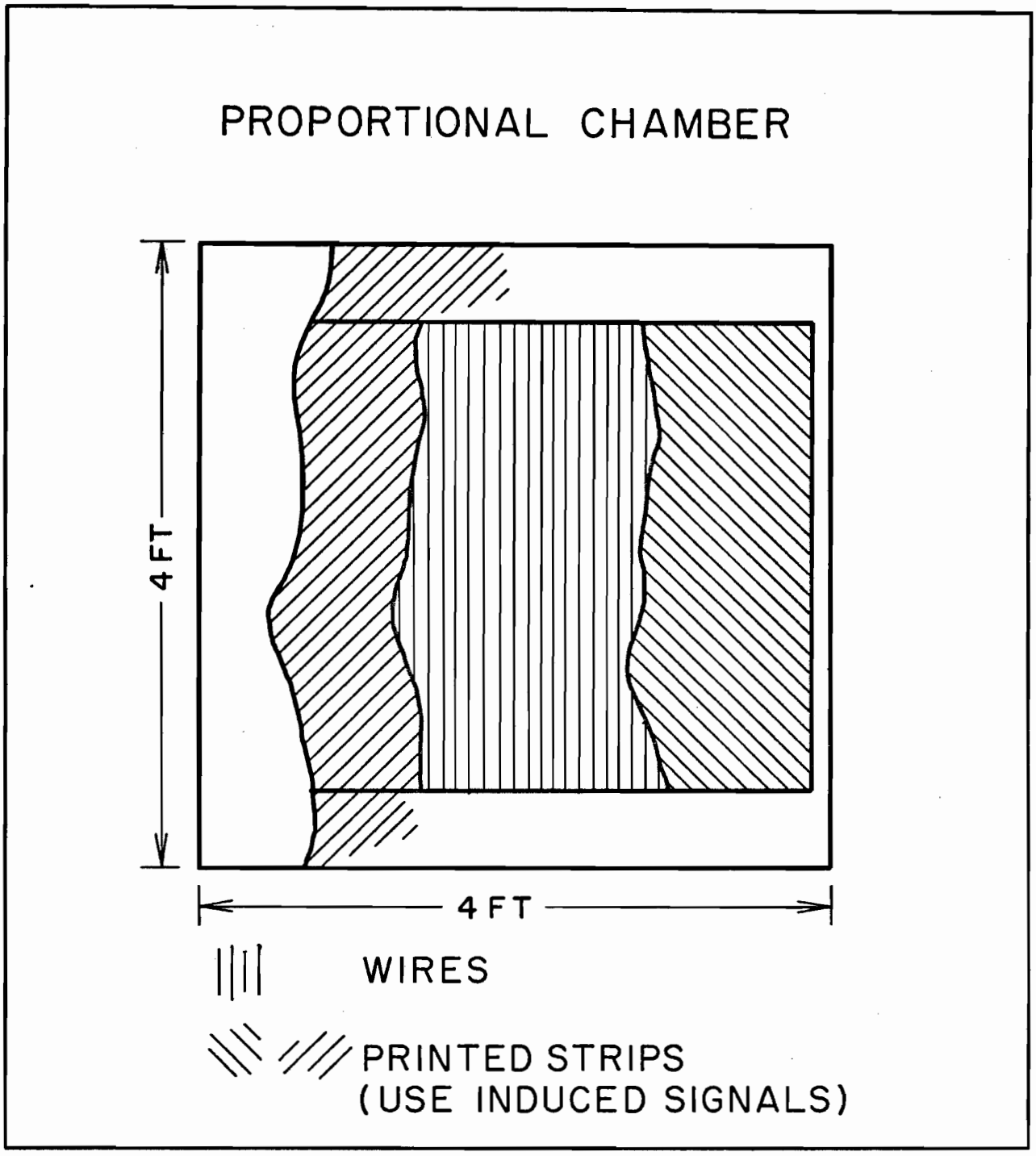
PROPORTIONAL CHAMBER
4 FT
4 FT
WIRES
PRINTED STRIPS
(USE INDUCED SIGNALS)

Figure 6

D. Backgrounds

The most important background is

$$\mu^+ N \to \mu^+ \pi^- X ;$$

$$\pi^- \to \mu^- \bar{\nu}_\mu .$$

The cuts which attenuate the effective cross-section for this process are first tabulated, then discussed:

Process and cut (cuts are cumulative)	Theoretical cross-section (pb)	Cross-section for simulated accepted and reconstructed data (pb)
Background:		
(1) $\mu^+ N \to \mu^+ X$; $E' < 100$ GeV	$2.3 * 10^5$	-
(2) $Q^2 > 3.7$ (GeV/c)^2	$7.7 * 10^3$	-
(3) $X = \pi^- + X'$; $\pi^- \to \bar{\nu}_\mu \mu^-$ (> 20 GeV)	$1.1 * 10^{-1}$	$1.1 * 10^{-1}$
(4) $p_\perp (\mu^-) > 1.4$ GeV/c	$1.5 * 10^{-3}$	$3 * 10^{-3}$
Data: $M_{M^o} = 4$ GeV		
(5) $\mu^+ N \to \bar{M}^o X$	$\gtrsim 1.1$	-
(6) $\bar{M}^o \to \mu^+ \mu^- \bar{\nu}_\mu$	$\gtrsim 2.7 * 10^{-1}$	$\gtrsim 1.2 * 10^{-1}$
(7) $E' (\mu^+) < 100$ GeV; $E' (\mu^-) > 20$ GeV; apparent $Q^2 > 3.7$ (GeV/c)^2; $p_\perp (\mu^-) > 1.4$ GeV/c	$\gtrsim 9.1 * 10^{-2}$	$\gtrsim 4.5 * 10^{-2}$

Background cross-section (2) was calculated assuming scaling and the Bloom-Gilman paramaterization[18] of νW_2, which was taken (pessimistically) as constant above $\omega = 20$. The main suppression factor of $7 * 10^4$ occurs between cross-section (2) and cross-section (3), which in addition requires a π^- to decay, within iron, to a μ^- of energy > 20 GeV. The input for obtaining this suppression factor is a Monte-Carlo calculation of

Riddell,[19] in which pions are produced by 200 GeV protons according to the Trilling formula, and decay into muons while cascading within solid copper. Let x be the ratio of muon energy to proton energy, and dN the number of muons in interval dx, per incident proton. Riddell found that

$$\frac{dN}{dx} < 6.4 * 10^{-3} * \exp(-18\,x)$$

for $x > 0.1$. We have used this result without change for incident virtual photons with energy between 100 and 200 GeV, and for pions cascading within the iron spectrometer.

A rough check on this suppression factor can be made by working backwards. Assume (in agreement with Riddell) that the effect of the hadron cascade is to multiply the muon flux by ≈ 2; and assume that muons with energy larger than 20 GeV come from pions which average 30 GeV in energy. The probability for 30 GeV pion decay within one interaction length (6 in) of iron is 10^{-4}. Therefore, adaptation of the Riddell result to this background problem is equivalent to setting the probability that a ~ 150 GeV virtual photon produces a π^- between (say) 25 and 40 GeV, equal to $1/(2 * 7 * 10^{4} * 10^{-4})$ or .07. This does not seem unreasonably small.

The final cross-section (4), requiring that the μ^- have a momentum transverse to the beam greater than 1.4 GeV/c, is smaller by an additional factor of 30. In this calculation, the π^- is given a (generous) distribution $e^{-3p_\perp^2}\, dp_\perp^2$ in momentum transverse to the virtual photon direction. The attenuation factor is half of that which would hold for an ideal apparatus.

The effect of these cuts on heavy lepton events at a typical lepton mass of 4 GeV is shown in cross-section (7). About 40% of the reconstructed data survive. The inequalities reflect the possibility (Table 1) that the $\bar{M}^o$ production cross-section exceeds the νN total cross-section, for $s \gg M^2_{M^o}$.

The result is reasonably model-independent. The μ^+ has large apparent Q^2 and the μ^- has large $p_\perp$ because the $\overline{M}^o$ is massive and is produced weakly, without a photon propagator. The μ^+ energy usually lies below 100 GeV, and the μ^- energy above 20 GeV, because the $\overline{M}^o$ energy is shared by its three daughters. We expect more sophisticated cuts, likelihood analyses, etc. to improve this survival rate in the final data analysis.

The result of this study is that $\pi^- \to \mu^- \bar{\nu}_\mu$ background is expected to comprise $\lesssim 7\%$ of the $M_{M^o} = 4$ GeV signal (comparing cross-sections (4) and (7), right-hand column). The signal/noise is even more favorable at higher heavy lepton masses, since the $\pi^- \to \mu^- \bar{\nu}_\mu$ suppression factor grows more rapidly than the event rate falls. The pion-decay background sets the lower limit on the range of M^o mass to which the experiment is sensitive. This lower limit is conservatively estimated to be 2 GeV.

We turn attention to other backgrounds. If every $\pi^+ \pi^-$ pair produced by a virtual photon were a ρ, the $\rho \to \mu^+ \mu^-$ contribution to the background would be a fraction of that from π^- decay. Also, K^- decay contributes less than the major background, for K/π ratios smaller than 0.5.

The effective cross-section for muon tridents, a smaller background than μ^+ - N scattering with $\pi^- \to \mu^- \bar{\nu}_\mu$ decay, has been roughly estimated. In an early experiment, Camac[20] found that 230-MeV electron bombardment of a 0.0045-in Cu foil resulted in an equal flux of 180-MeV positrons from direct- and photo-pair production. Half this thickness, corrected slightly for the case of 200 GeV incident muons ($\gamma \approx 2000$ instead of $\gamma \approx 500$), corresponds to an "equivalent radiator for muon-trident production" of .004 radiation lengths. In μ-trident diagrams like this,

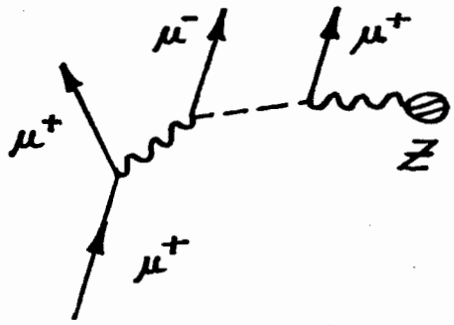

a Weizsacker-Williams flux of .003 > 100-GeV virtual photons per 200 GeV muon is thereby available for Bethe-Heitler-like production of muon pairs. The cross-section for the latter process is less than that for muon-pair production by real photons, as calculated by Kim and Tsai.[9] A numerical integration of the Kim-Tsai results for 200 GeV photons on Be yields a total muon-pair-production cross-section of 10^{-34} cm^2/nucleon, for μ^- transverse momenta exceeding 1 GeV. Using a factor-of-3 enhancement for coherence in Fe vs. Be, one obtains a total μ-trident cross-section $\lesssim$ 1 pb/nucleon in Fe, with the above restrictions on μ^- transverse momentum and μ^+ energy loss.

For the trident to mock a pair, one μ^+ must not be detected. The probability of either μ^+ being softer than the minimum-detectable 5 GeV is only 7%. To allow for instrumental effects, we double that inefficiency. The resulting effective cross-section is $\lesssim$ .14 pb, about twice the signal.

Finally, the μ-trident background is suppressed by two additional large factors. First, as Tannenbaum has pointed out,[21] in all μ-trident diagrams <u>two</u> propagators can be forced far off-shell by requiring large μ-pair mass; and large momentum of the pair <u>and</u> the μ^+, transverse to the beam direction. Enforcement of these requirements at the 1-GeV/c transverse-momentum level introduces an extra suppression factor of at most $(2m_\mu/p_\perp)^2 \approx .05$. Second,

μ-trident production involves negligible energy transfer to hadrons and electrons. In contrast, 4-GeV M^o production typically is accompanied by an 80-GeV hadron shower, satisfying the trigger requirement, whereas essentially all μ-trident data will be suspiciously clean. Evidently, μ-trident background can be made negligible, by at least 2 orders of magnitude.

In analyzing the data, the effect of cuts on background processes will be determined experimentally. Here one uses the fact that $\mu^+\mu^-$ events of the major background types have $\mu^+\mu^+$ analogues. Evidence for existence of the M^o, if any, would consist of a large excess of $\mu^+\mu^-$ events over $\mu^+\mu^+$ events, after background cuts. In the case of a null result, Monte Carlo calculations of the (reasonably model-independent) effect of these cuts will determine the experiment's sensitivity.

Finally, we mention accidentals. The potentially most bothersome effect is a three-fold accident involving (1) two unresolved beam muons (probability $\lesssim 10^{-3}$); (2) scattering of one muon with $Q^2 > 3.7$ $(\text{GeV/c})^2$ and $\nu > 100$ GeV (probability $\approx 3 * 10^{-5}$); (3) mismeasurement of a 200 GeV μ^+ as a μ^- of less than 100 GeV (probability $\lesssim 10^{-4}$). The combined accidental rate is smaller than the event rate by more than 3 orders of magnitude.

To sum up, background suppression is not difficult, except for the major effect, μ^+ - N scattering with $\pi^- \rightarrow \mu^- \bar{\nu}_\mu$ decay. To cut out this process with an adequate margin of safety, one needs to produce and detect the final-state particles within continuous dense material, in order to force the pions to interact before decaying.

E. Event Rates and Conclusion

The following table gives the number of detected M^o events per experiment (10^{12} 200 GeV muons), for various M^o masses. Allowance has been made for $M^o \to \mu^+\mu^-\nu_\mu$ branching ratio (25%), apparatus acceptance (50%), and survival rate after background cuts (40% at $M_{M^o} = 4$ GeV).

M^o mass (GeV)	Events	Remarks
2	$\gtrsim$ 120 ?	Depends on background subtraction.
4	$\geq$ 200	Full calculation.
6	$\gtrsim$ 190	Full calculation except for estimate of survival rate after background cuts.
8	$\gtrsim$ 120	
10	$\gtrsim$ 60	

The inequalities become equalities if

$$\sigma(\mu^+ \text{ (L.H.) } N \to \bar{M}^o X) = \sigma(\nu N \to \mu^- X)$$

in the limit $s >> M^2_{M^o}$, as is roughly true in the least optimistic gauge theories (Table 1).

After allowance for contingencies and backgrounds, we conclude that this experiment can unequivocally establish the existence or non-existence of neutral heavy muons predicted by gauge theories, having mass between 2 and 10 GeV.

III. OTHER EXPERIMENTS

The possibilities for measurements concurrent with the M^{o} search are especially rich. In no other type of beam can one measure nucleon charge structure, test QED, and explore weak processes at once.

A detailed discussion of the most interesting and feasible of these experiments will be submitted as an addendum to this proposal. At this point, we shall only mention properties of the proposed spectrometer which make possible the achievement of new experimental goals. These properties are:

1. A massive target -- 30 ft of Fe -- has $\sim$ one order of magnitude more nucleons/cm^2 than can be used in other muon experiments. For a 10^{12}-muon run, the sensitivity of the experiment to rare processes, before efficiencies are folded in, is 4000 events per picobarn.
2. Large angular acceptance (>50 msr) is achieved by distributing the measuring planes through the target. More important, there is no minimum scattering angle required for acceptance: the good time resolution of the proportional chambers makes it unnecessary to deaden their sensitivity in the beam area. The latter feature is crucial to the ability to detect all the muons in a multi-muon final state.
3. Flexible tolerance on beam quality is another benefit derived from use of proportional chambers. In calculations, we have assumed an 8 by 10-in beam area, and have required only that the beam and the halo outside that region have intensity $\lesssim$ 10 MHz. This flexibility makes it reasonable to envision substantial periods of compatible data-taking downstream of the Muon Scattering Facility.

With these benefits, the proposed spectrometer has resolution and ease of triggering sufficient for a number of applications. For muons arising from M^{o} decay, averaging 50 GeV in energy, the energy resolution is $\pm$10.5%, typical of iron-magnet spectrometers. This figure improves if the information in the two proportional chambers just downstream of the vertex is not masked by a hadron shower; or if the muon penetrates more than 7-9 magnets while remaining within the active area of the magnets and chambers. Because the measuring planes are distributed through the target, the muon is detected after Coulomb scattering in only a small fraction of the target thickness. For muons produced forward, the resolution in projected transverse momentum at the production point is $\pm$150 MeV/c. For muons produced with transverse momentum exceeding 2 GeV/c, the uncertainty in transverse momentum is dominated by the energy resolution.

As for triggering, the large thickness of iron in the spectrometer makes it feasible to use the shower developed there to identify a muon interaction with appreciable energy transfer to hadrons. The trigger rate is reduced to a manageable level by requiring, in addition, (1) a multiple muon signal downstream, and/or (2) a minimum muon scattering angle, depending on the reaction being studied.

To conclude, we expect that the strengths of the spectrometer proposed here make possible a number of new measurements of significant interest, which, in particular, are truly complementary to the program of the Muon Scattering Facility.

REFERENCES

1. A. Salam and J. E. Ward, Phys. Letters 13, 168 (1964); G. 'tHooft, Nucl. Physics B35, 167 (1971); and Refs. 2, 4-6.

2. S. Weinberg, Phys. Rev. Letters 19, 1264 (1967) and 27, 1688 (1971); Phys. Rev. D5, 1412 (1972) and D5, 1962 (1972).

3. D. H. Perkins, Review Paper given at the XVI International Conference on High Energy Physics, Chicago-Batavia (Sept. 5-13, 1972), Oxford University preprint.

4. J. D. Bjorken and C. H. Llewellyn Smith, Phys. Rev. D7, 887 (1973).

5. B. W. Lee, Phys. Rev. D6, 1188 (1972); J. Prentki and B. Zumino, Nucl. Phys. B47, 99 (1972).

6. H. Georgi and S. L. Glashow, Phys. Rev. Letters 28, 1494 (1972); Phys. Rev. D7, 561 (1973).

7. J. R. Primack and H. R. Quinn, Phys. Rev. D6, 3171 (1972).

8. W. Lee et al., "Proposal to Search for Heavy Leptons and Intermediate Bosons from Photon-Nucleon and Photon-Nuclei Collisions," NAL Proposal No. 87 (1970).

9. K. J. Kim and Y. S. Tsai, preprint SLAC-PUB-1105 (1972).

10. L. W. Mo et al., "Status Report on the Muon-Nucleon Scattering Facility at the National Accelerator Laboratory" (Sept. 14, 1972), and NAL Proposal No. 98 (1970).

11. C. H. Albright, Phys. Rev. Letters 28, 1150 (1972).

12. K. W. Chen and L. N. Hand, "High Momentum Transfer Inelastic Muon Scattering and Test of Scale Invariance at NAL," NAL Proposal No. 26 (1970).

13. B. Barish et al., "Neutrino Physics at Very High Energies," NAL Proposal No. 21 (1970).

14. Y. Kang et al., Particle Accelerators 4, 31 (1972).

15. V. L. Fitch, V. Hepp, D. A. Jensen, M. Strovink, and R. C. Webb, BNL-AGS Experiment No. 540 (1971) (to be published).

16. M. L. Stevenson et al., "Proposal to Develop a Phase I External Muon Identifier (EMI) for Use with the NAL 30 m^3 Bubble Chamber," NAL Proposal No. 155 (1971); M. L. Stevenson, private communication.

17. A. Browman, private communication.

18. E. D. Bloom and F. J. Gilman, Phys. Rev. Letters 25, 1140 (1970); G. Miller et al., Phys. Rev. D5, 528 (1972).

19. R. J. Riddell Jr., UCRL-11989 (1965), unpublished. We use the result of this report reproduced in Fig. 3 of D. Keefe and C. M. Noble, Nucl. Inst. and Meth. 64, 173 (1968).

20. M. Camac, Phys. Rev. 88, 745 (1952).

21. M. J. Tannenbaum, Phys. Rev. 167, 1308 (1968).

22. D. R. Harrington, Phys. Rev. 120, 1482 (1960).

23. T. Yamanouchi, private communication.

24. L. N. Hand and M. Strovink, "Will the N.A.L. Muon Beam Meet Original Specifications?", NAL report (1971).

25. T. A. Nunamaker, Rev. Sci. Instr. 42, 1701 (1971).

APPENDIX A

Production and Decay of the M^o

1. Production

In the limit of negligible muon mass, invariance to isospin rotation gives

$$\sigma\ (\mu^-\ (\text{L.H.})\ N \to \nu_\mu\ X) = \sigma\ (\nu_\mu\ N \to \mu^-\ X), \tag{1}$$

if N is an average of proton and neutron. Also, for negligible M^o mass,

$$\sigma\ (\mu^-\ (\text{L.H.})\ N \to M^o\ X) = (g_L^{\,2}/g^2)\ \sigma\ (\mu^-\ (\text{L.H.})\ N \to \nu_\mu\ X), \tag{2}$$

where $g_L^{\,2}/g^2$ is the ratio of the left-handed weak coupling strengths for M^o and ν_μ. Finally,

$$\sigma\ (\mu^+\ (\text{L.H.})\ N \to \overline{M}^o\ X) = (g_R^{\,2}/g_L^{\,2})\ \sigma\ (\mu^-\ (\text{L.H.})\ N \to M^o\ X), \tag{3}$$

where $g_R^{\,2}/g_L^{\,2}$ is the ratio of abnormal-helicity to normal-helicity weak coupling strength of the M^o. The latter equality is the result of two changes in the sign of the vector-axial vector interference term: one from the lepton → antilepton transition, and one from the transition from normal to abnormal helicity. Combining (1), (2), and (3), we have, except for effects of finite lepton mass,

$$\sigma\ (\mu^+(\text{L.H.})\ N \to \overline{M}^o\ X) = (g_R^{\,2}/g^2)\ \sigma\ (\nu_\mu\ N \to \mu^-\ X).$$

The factor $g_R^{\,2}/g^2$ has a value $\gtrsim 1$ for the gauge theories enumerated in Table 1.

The cross-section for $\nu\ N \to \ell^-\ X$ may be written <u>without</u> neglecting the lepton mass as [11]

$$\frac{d^2\sigma}{dy\ dz} = \frac{G^2\ E\ M}{\pi}\frac{1}{y}\left\{y^2\ (1 + \ell/z)\ F_1/\omega + \left[1 - y - z\ (1 + \ell/z)\ (M/2\ E)\right] F_2\right.$$

$$\left. - y\left[1 - y/2\ (1 + \ell/z)\right] F_3/\omega + y\ell\ (1 + \ell/z)\ F_4/\omega - \ell\ F_5\right\} \quad ,$$

where

ν = energy transferred to hadrons,
E = incident lepton energy,
Q^2 = (momentum transfer)^2 to hadrons,
M = nucleon mass,
m = heavy lepton mass,
y = ν/E,
ℓ = m^2/s,
ω = $2M\nu/Q^2$,
z = Q^2/s,

and F_1 through F_5 are the nucleon structure functions. The well-satisfied Callan-Gross relation sets $2F_1/\omega = F_2$, and the observation[3] that $\sigma_T^{\bar{\nu}}/\sigma_T^{\nu} \approx 1/3$ suggests that $F_3/\omega = -F_2$. Because F_4 and F_5 are multiplied by the lepton mass, they contribute negligibly to the $\nu_\mu\ N \to \mu^-\ X$ cross-section, so have not been measured. We have set F_4 and F_5 to zero (a speculation not in disagreement with spin-1/2 parton models), thereby introducing uncertainty in the cross-section at the factor-of-2 level.

With these choices, the $\bar{M}^o$ production cross-section becomes

$$\frac{d^2\sigma\ (\mu^+\ (\text{L.H.})\ N \to \bar{M}^o\ X)}{dy\ dz} = \frac{g_R^2}{g^2}\frac{G^2\ E\ M}{\pi}\frac{F_2\ (\omega)}{y} \qquad (4)$$

where M has been neglected relative to E. This expression is independent of lepton mass, except for kinematic restriction of the allowed area in the Q^2 - ν plane (Fig. A1). Another feature of (4) is a flat ν/E distribution,

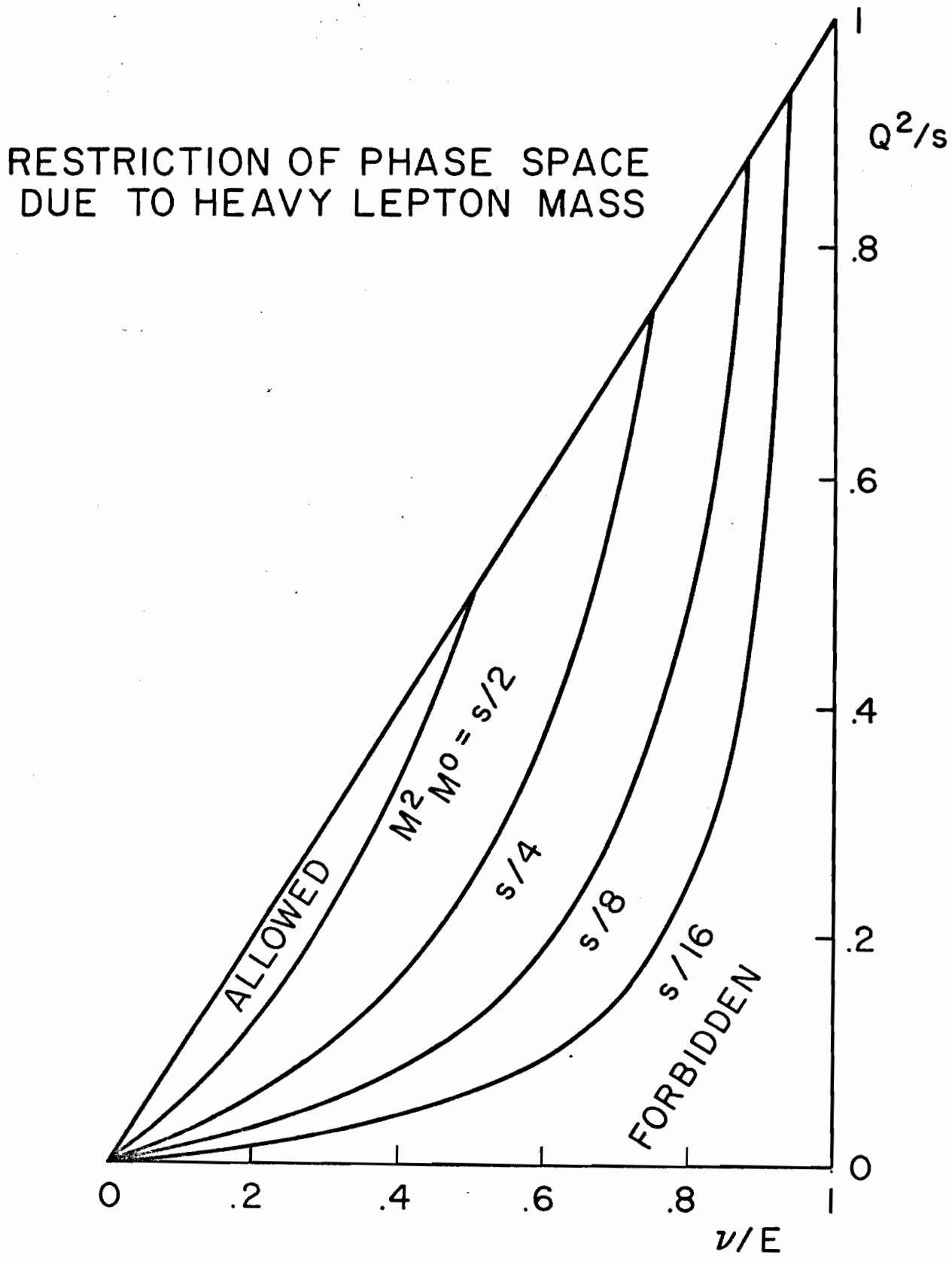
RESTRICTION OF PHASE SPACE
DUE TO HEAVY LEPTON MASS
Q^2/s
1
.8
.6
.4
.2
0
ALLOWED
$M^2 M^0 = s/2$
s/4
s/8
s/16
FORBIDDEN
0
.2
.4
.6
.8
1
ν/E

Figure A1

after integration over Q^2, in the case of negligible lepton mass. In computations we have set

$$F_2^{(\nu N)}(\omega) = 4\ \nu W_2^{(\gamma N)}(\omega)$$

For $\nu W_2^{(\gamma p)}$ we have assumed scaling and used the Bloom-Gilman[18] parameterization; $\nu W_2^{(\gamma n)}$ has been equated to $\nu W_2^{(\gamma p)}\left[1 - 3/(4\omega)\right]$.

A Monte Carlo routine, using the above information, has reproduced the expected Q^2 - ν plane distribution for $\nu_\mu\ N \rightarrow \mu^-\ X$. Numerical integration has given the usual $0.8 * 10^{-38}\ cm^2 * E\ (GeV)$ total cross-section. The calculated relative cross-section at non-negligible lepton mass is superimposed, in Fig. A2, on the same quantity calculated by Bjorken and Llewellyn Smith.[4] In view of the approximations, the agreement is good.

It is worth commenting on the extent to which the usual notion of scaling is extrapolated in order to obtain these cross-section estimates. We have remarked that, at $M_{M^o} = 4$ GeV, an average Q^2 of only 35 $(GeV/c)^2$ is transferred to the target nucleon; thus, the extrapolation of "pointlike" nucleon structure is reasonably short. If there should exist a W propagator which significantly attenuates the assumed linear rise to 200-GeV ν energy of the ν - N cross-section, the W would be much less massive than in all gauge theories except for the Georgi-Glashow version. In the latter case, however, the decrease in the ν - N cross-section would be more than compensated by the $1/M_W^{\ 2}$ dependence of $g_R^{\ 2}/g^2$.

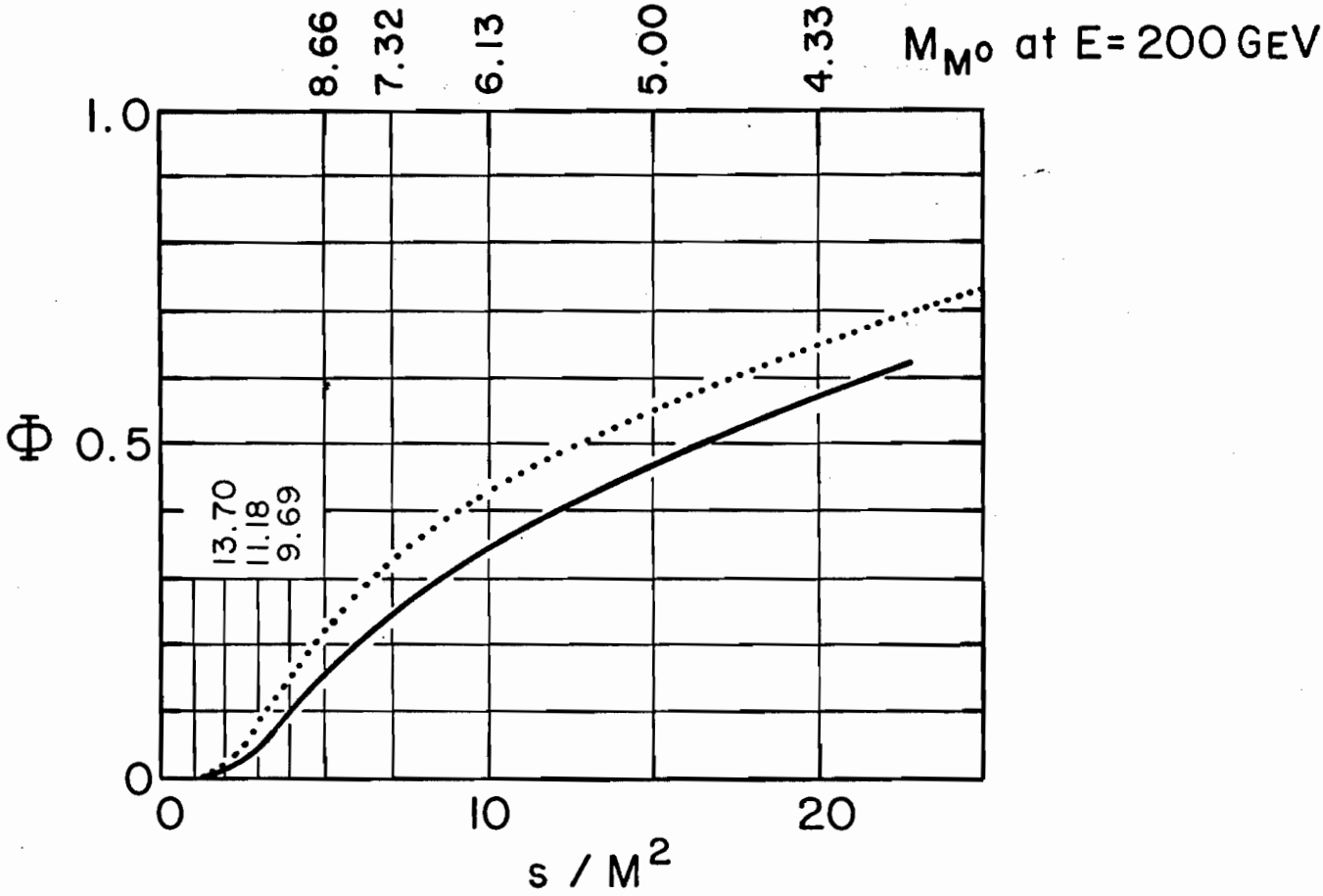

Figure A2

The ratio Φ of production cross-section in μ^+N collisions of finite-mass $\bar{M}^o$, to production cross-section of zero-mass $\bar{M}^o$, as a function of s/M^2_{Mo}.

———————— Bjorken and Llewellyn Smith (Ref. 4)

..... Monte Carlo calculation - this proposal

2. Decay

The differential decay rate for

$$\bar{M}^o \to \mu^+ \mu^- \bar{\nu}_\mu ,$$

where the $\bar{M}^o$ couples to the μ^+ with a (V + A) current, was obtained by analogy with the general expression[22] for the differential decay rate for

$$\Lambda \to p\, e^- \bar{\nu}_e .$$

In both decays the masses of the final-state particles were set to zero. To obtain the desired (V + A) coupling, the general expression for the Λ decay rate was specialized to the case of a hadronic weak current with $g_A = + g_V$ as the only nonzero couplings. The result is

$$\frac{d^5 \Gamma (\bar{M}^o \to \mu^+ \mu^- \bar{\nu}_\mu)}{dx_{\mu^-}\, dx_\nu\, d\Omega_\nu\, d\varphi_{\nu\mu^-}} \propto x_\nu (1 - x_\nu) (1 + P \cos \theta_\nu) , \qquad (5)$$

where

$$x = 2\, p_{C.M.}/M_{M^o} ,$$

θ_ν and φ_ν pertain to the C.M. $\bar{\nu}_\mu$ direction relative to the $\bar{M}^o$ direction, $\theta_{\nu\mu^-}$ and $\varphi_{\nu\mu^-}$ pertain to the C.M. μ^- direction relative to the $\bar{\nu}_\mu$ direction, and P is the $\bar{M}^o$ polarization along its direction of motion. The decay rate, differential in these variables, depends only on the C.M. energy and direction of the neutrino, which is the final-state particle of unlike helicity. As a check, notice that the rate for an $\bar{M}^o$ with $P \approx 1$ decaying into a forward neutrino near maximum energy, is suppressed by two factors which are nearly zero. This is expected because the total spin component in the $\bar{M}^o$

direction of motion would differ, between the initial and final state, by two units.

A Monte Carlo routine, based on Eq. (5), was checked by integrating over the neutrino variables. The resulting energy-angle distribution of the μ^- was the same as the usual expression for the e^- in polarized μ^- decay. If, as one might expect, the $\overline{M}^o$ carries the left-handed polarization of the incident μ^+, the muons are emitted preferentially forward and with high C.M. energy. The corresponding laboratory muon energy averages 40% of the total. For this choice of $\overline{M}^o$ polarization, apparatus acceptance and background rejection are maximized. In the simulations, we instead have assumed that the $\overline{M}^o$ has right-handed polarization. This reduces the average muon energy by 25%, and amounts to a worst-case assumption.

APPENDIX B

Reconstruction of Simulated Events

We first describe a general procedure for reconstructing single muon tracks in magnetized iron. Then we discuss its extension to the case of two muons in the final state, originating at a common vertex.

To make optimal use of the available information, one can make a simultaneous least-squares fit to the free parameters describing the muon track. In the bending plane, these are the transverse position y_o and direction tangent s_o of the muon at the coordinate along the beam axis of the interaction point, and the muon momentum $p_o = 1/\rho_o$, projected in that plane. An immediate complication arises in attempting to assign a standard deviation σ_i to the n transverse position measurements Y_i, interspersed between N regions of magnetized iron. The problem is that a sizable component of the measuring error is due to multiple Coulomb scattering in the iron, giving correlated shifts in the measured positions. Our approach to this difficulty was to introduce N additional free parameters d_j, equal to the projected transverse momentum impulse due to multiple Coulomb scattering in each of the N magnet segments. Correspondingly, one had N additional "measurements" $d_j = 0 \pm e_j$, where e_j is the rms value of d_j appropriate to the thickness of the iron segment. With introduction of these new parameters, the σ_i became the deviations due only to intrinsic chamber measuring error.

Each magnet was taken to impart an impulse q_j of transverse momentum to the muon. This was iteratively corrected for departure from normal muon incidence. Also, the measured transverse coordinate Y_i was given an iterative correction ΔY_i for the effect of muon energy loss, or gain $\Delta\rho_j$ in inverse momentum, in each magnet. To summarize, the full chi-square became

$$\chi^2 = \sum_{i=1}^{n} \frac{[y_i - (Y_i + \Delta Y_i)]^2}{\sigma_i^2} + \sum_{j=1}^{N} \frac{d_j^2}{e_j^2} ,$$

where

$$y_i = y_o + s_o z_i + \sum_{\substack{j=1 \\ w_j<z_i}}^{N} (z_i - w_j)(q_j \rho_o + d_j \rho_j) ;$$

$$\Delta Y_i = \sum_{\substack{j=1 \\ w_j<z_i}}^{N} (z_i - w_j) q_j \Delta\rho_j ;$$

z_i and w_j are the coordinates along the beam axis, relative to the vertex, of the measuring planes and magnet segment midpoints; and $\Delta\rho_j$ and $\rho_j = \rho_o + \Delta\rho_j$ are determined from the value of ρ_o obtained in the previous iteration. The best fit to the free parameters y_o, s_o, ρ_o, and $(d_1, \cdots, d_N)$ was obtained by solving the $(N + 3)$ simultaneous linear equations

$$\frac{\partial\chi^2}{\partial y_o} = \frac{\partial\chi^2}{\partial s_o} = \frac{\partial\chi^2}{\partial\rho_o} = \frac{\partial\chi^2}{\partial d_1} = \cdots = \frac{\partial\chi^2}{\partial d_N} = 0.$$

This procedure for reconstructing a single muon track in the bending plane was generalized to 3-dimensional reconstruction of the two muon daughters of the $\overline{M}^o$, in the following way. Initially, a hypothetical vertex coordinate z_v along the beam direction was chosen, and the transverse vertex position determined by the intersection of the primary muon track with the $z = z_v$ plane. Each secondary muon track was required to intersect this vertex point. For each of the secondary tracks, the bending-plane reconstruction procedure described above was applied. Subsequent recon-

struction in the orthogonal plane proceeded in a similar way, except that ρ_o was fixed by the bending-plane reconstruction, and the q_j became zero. An overall χ^2 corresponding to the particular choice of z_v was computed. Then, z_v was varied, and the procedure repeated to obtain new χ^2 values for different choices of longitudinal vertex coordinate. A best-fit z_v was obtained using a combination of a binary search, and a polynomial fit to the χ^2 for vertex coordinates near the optimum. For this best-fit z_v, the reconstruction procedure was repeated a final time, to obtain the best-fit parameters of the event.

As implemented on the Princeton 360/91 for the spectrometer described in Part II, the algorithm required ~ 100 msec of CPU time per event. The routine was checked in two ways, using simulated events generated by a completely independent Monte Carlo program. In the first check, "perfect" Monte Carlo events, with all dispersive mechanisms turned off, were reconstructed essentially exactly. In the second check, the program reconstructed simulated events with all non-Gaussian dispersive mechanisms (μ bremsstrahlung, energy loss straggling from μ - e scattering, Molière scattering) turned off. A chi-square distribution was obtained which matched the standard prediction for the appropriate number of degrees of freedom.

APPENDIX C

Muon Beam Intensity

At muon energy/proton energy of 100 GeV/200 GeV, NAL has achieved[23] a peak muon/proton yield of $0.6 * 10^{-8}$. This is 20% of the yield predicted by the first realistic simulation[24] of the NAL muon beam. It is assumed that, if the beam components were to remain unchanged, adiabatic improvements in proton beam emittance, extraction stability, and alignment of various elements in the neutrino target hall would raise the average yield at least to this peak value.

In addition, the following minor beam improvements can be contemplated:

Improvement	Estimated gain in intensity
Encl. 101 aperture: 2 x 3 in → 4 x 4 in	x 3.0
Encl. 104 aperture: 2 x 4 in → 4 x 4 in	x 1.5
Put 3Q84's in Encl. 100	x 1.8
Improved vertical trimming and alignment downstream of absorber	x 1.2
Total	x 10

It has long been known that the existing "trainload", which momentum-selects hadrons for the dichromatic neutrino beam, produces a beam spot which is badly matched to the muon beam aperture. A simple doublet or triplet lens with aspect ratio near unity would increase the muon intensity by a factor of at least 7, by our calculation. Depending on the needs of the neutrino program, such a lens could be folded into a dichromatic arrangement, or used in a horn bypass.

Finally, by our estimate, doubling the muon/proton energies to 200 GeV/400 GeV will at least double the muon yield.

All told, it is evident that a yield of $\sim 10^{-6}$ 200 GeV muons/400 GeV proton can be achieved with no new construction or major financial commitment by NAL, although it will be necessary for the laboratory to develop the beam. With this yield, the required 10^{12} muons correspond to 10^{18} protons. At $2 * 10^{13}$ protons/6 sec on target, the integrated muon flux required by this experiment could be produced in 80 hours.

Because of trigger-rate limitations, however, this experiment is designed for a maximum μ intensity of 10 MHz. With 0.5 sec effective spill length, this means that the 10^{12} muons would be delivered with at most $5*10^{6}$/pulse, over at least 330 hours.

APPENDIX D

Proportional Chamber Electronics

We are proposing to build 18726 channels of single-wire proportional-chamber readout, costing $ 2.50 per channel. An electronics design will be finalized as the experiment moves from proposal to construction stage. At this point, we want to outline the design considerations, with emphasis on ideas which make the low cost possible.

Because of low cost, TTL logic must be used. We begin with the back end of the circuit and work forward. Experience with single-wire spark-chamber readout[25] has established the parallel-in serial-out 8-bit shift-register as the optimum information storage element, at $\lesssim 20¢$/bit. Browman[17] has devised a pre-latching arrangment using 1/4 of a 7408, which makes it possible to vary the coincidence width without changing components. The delay before coincidence must be created by a one-shot, rather than by a more expensive passive element. To reduce consumption of power and funds, the usual TTL one-shot may be replaced with a cruder circuit. Browman has used another 1/4 of a 7408, which requires individual trimming. Alternatively, one can introduce capacitively-coupled positive feedback around the amplifier section. In either case, the one-shot width can be made sensitive to variation in input pulse height, in a way which partly cancels the time-slewing due to that variation.

At present there is no completely satisfactory amplifier circuit. Browman's amplifier has 15 discrete components. Alternatively, the cheapest integrated circuit with adequate gain bandwidth is the 72810, expensive at 50¢. To obtain additional sensitivity ($\sim$ 1/3 mV) for pickup of induced pulses, we have tested a gain-of-20 preamplifier which uses 1/6 of a 74L04 inverter.

Figure D1 is the schematic of a circuit we have prototyped, which incorporates the 74L04 preamplifier, 72810 amplifier/one-shot, and shift-register coincidence and readout. It has fixed coincidence width. Figure D2 is a layout of 48 of these circuits for an application requiring minimum circuit board width per channel. The relaxed spatial constraints in this experiment will make it possible to eliminate the long input leads. We expect that a combination of this and Browman's design will meet the cost and performance criteria.

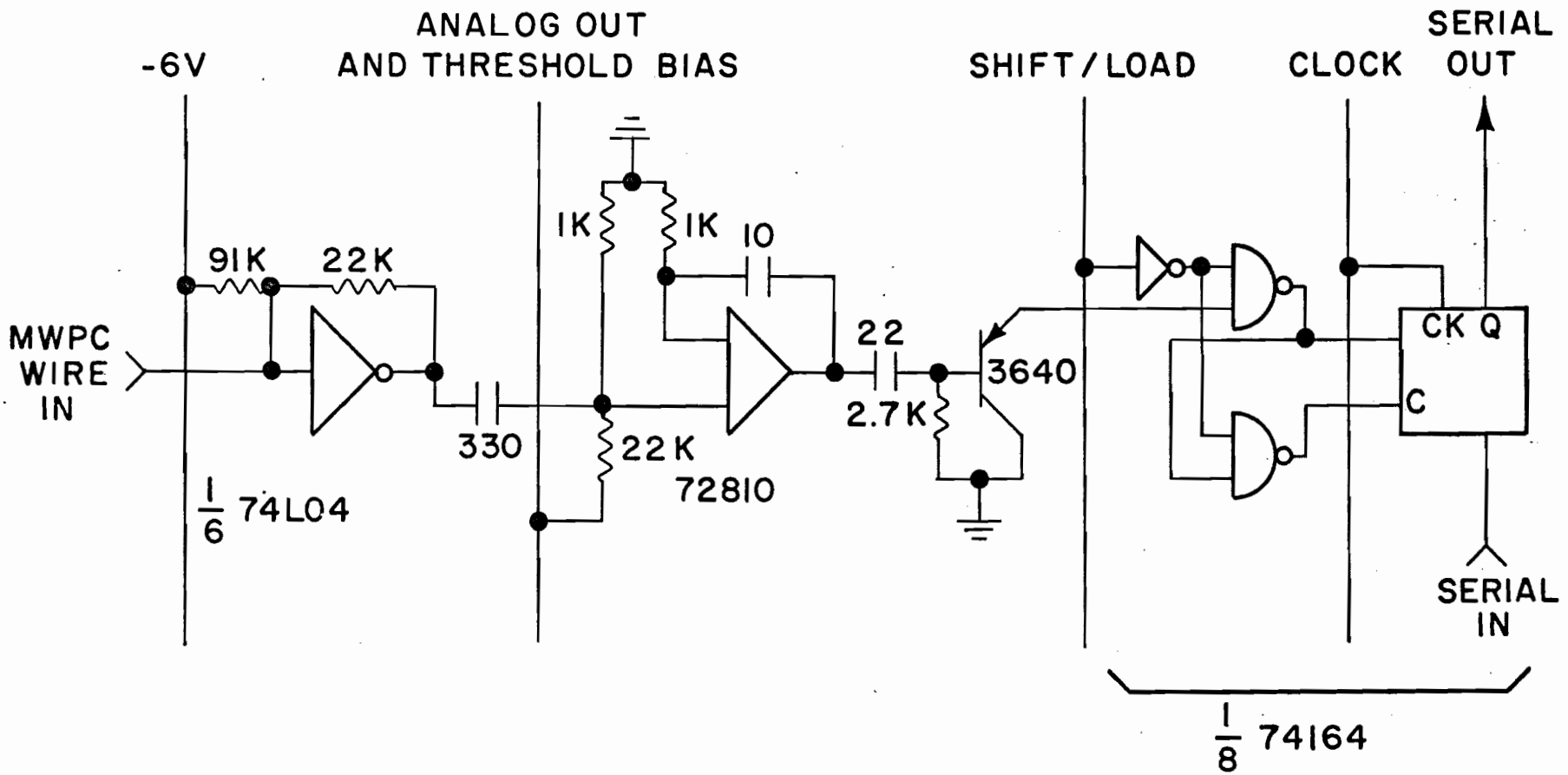
POSSIBLE MWPC ELECTRONICS
-6V
ANALOG OUT
AND THRESHOLD BIAS
SHIFT/LOAD
CLOCK
SERIAL
OUT
MWPC
WIRE
IN
91K
22K
1K
1K
10
330
22K
72810
22
2.7K
3640
CK Q
C
SERIAL
IN
1/6 74L04
1/8 74164

Figure D1

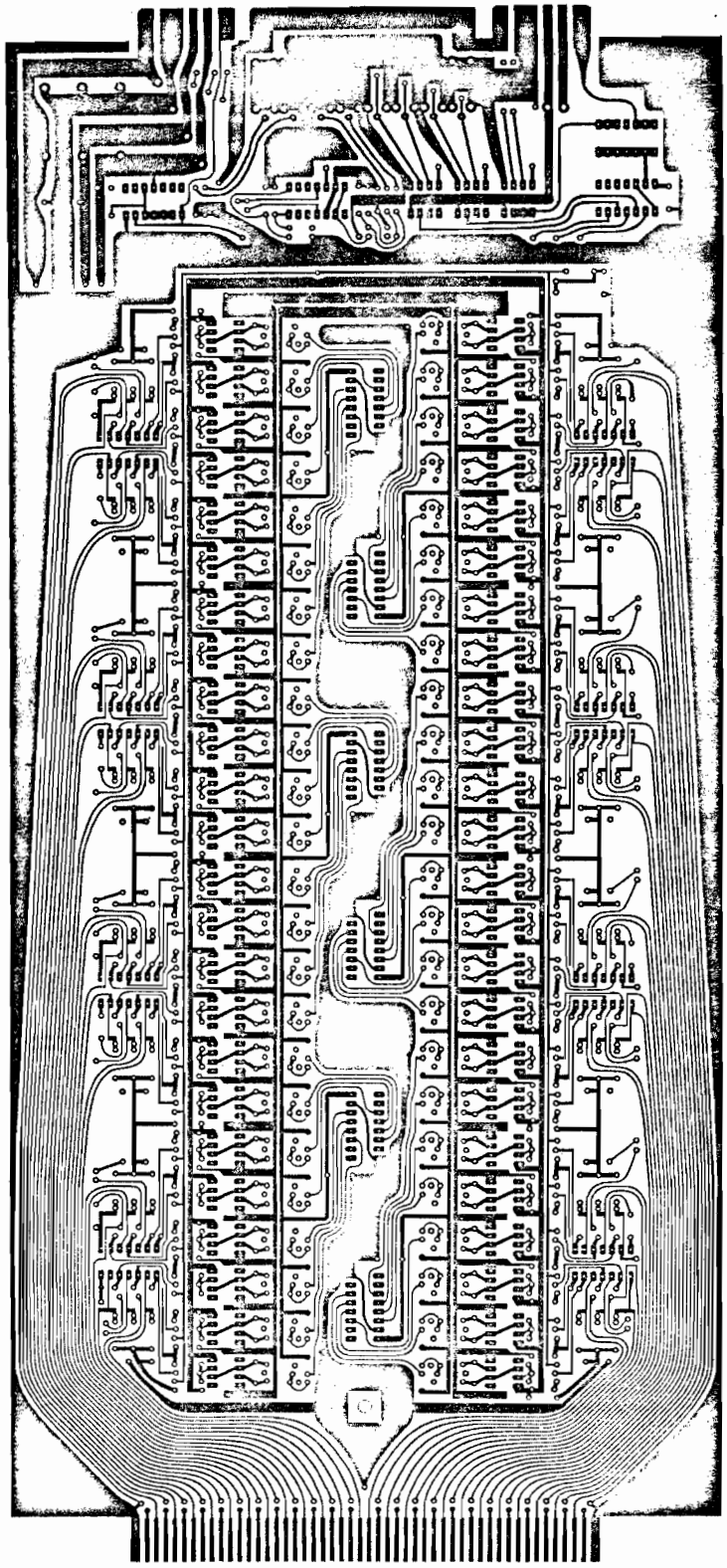

Figure D2

APPENDIX E

Magnet Construction

The precision required of the iron slabs is such that shaping by flame cutting is adequate. The requirements on the magnetic properties would allow them to be fabricated from reject low-carbon steel plate, available from mills near NAL. The winding slots, as well as the outside edges are flame-cut, and then the plates tack-welded into slabs 2 ft thick. After all 25 slabs are arranged in the Muon Laboratory, a single coil is wound through all the slots. There are thus only two places where the coil is transverse to the beam, resulting in a large reduction in the total length of the winding.

For a B field in the iron of 18.5 kG, H is about 200 Oersteds. With the dimensions shown in Fig. 4 this field is reached with 90,000 ampere turns. Since the width of a coil window adds little to the amount of iron, it seems natural to choose aluminum conductors. A possible choice would be rectangular aluminum bars, 3/4 in high by 1-1/2 in wide, with a 1/2-in diameter water cooling hole. The winding slots would then accomodate 41 turns in a single stack with the result that the current could be 2200 amperes. The total resistance would be 72 milliohms and the power 330 kW. The total weight of conductor, with these dimensions, is 5900 lbs. Without good figures on unit costs, one cannot estimate closely, but this choice of dimensions appears to give a reasonable balance between the cost of the coil and the cost of the power supply. Of course, these preliminary conductor dimensions can be adjusted to properly match available power supplies, or to optimize the total cost of power supplies and windings.

We imagine that the coil bars would be insulated with epoxy impregnated glass sleeving cured in advance of winding, and that the bars would then be

inserted into the slots. The water connections would be aluminum hose bibs welded on in advance. The cross-connections at the ends could either be welded in the field or clamped. The soft aluminum bars with these dimensions would be easily bent after installation to provide space to make the connections. It should be noted that the magnetic forces on the conductors are negligible in a magnet such as this without airgap. There is nothing to be gained by compact end connections. Insulation of the cross-connections at the ends of the spectrometer can be easily and adequately done in the field.

APPENDIX F

Equipment

Detectors. We anticipate that the multiwire proportional chambers, multiwire proportional chamber electronics, and scintillation counters would be designed and constructed at Princeton. The total cost of multiwire proportional chambers and electronics is estimated at $73K. Most of the ~ 100 scintillation counters can use inexpensive phototubes. We have not yet determined the level of new expenditure which these counters represent. We would expect fast logic for these counters to be supplied by PREP.

Assuming that the level of funding of the Princeton AEC research contract does not significantly change, it should be possible to construct these detectors without supplemental funds. This is made possible by the fact that the three experiments to which the group presently is committed have nearly all of their required apparatus completed and installed.

On-line Computer. Use of a PDP-11 or similar small computer is essential. It is possible that a Princeton computer will become available.

Magnets. The magnets are estimated to cost $67K. Without supplemental allocation for this purpose, the cost of magnet construction and installation cannot be borne by Princeton. However, we are prepared to assume full responsibility for all aspects of the magnet design.

APPENDIX G

Scientific Personnel

The proponents of this experiment are:

Cyrus M. Hoffman, Assistant Professor

(presently involved in BNL-AGS Experiment 548)

Rosanna Cester Regge, Visiting Associate Professor

(presently involved in CERN-PS Experiment P9)

Frank C. Shoemaker, Professor

(presently involved in BNL-AGS Experiment 548)

Mark Strovink, Assistant Professor

(presently involved in NAL Experiment 26)

All of the above-named experiments are in the data-taking or analysis stage. The group expects to add to its strength by attracting additional Princeton collaborators.

At various times, responsibility for communication with NAL will fall upon one or another of the group members. At present, the correspondent is M. Strovink.

Addendum to NAL Proposal 203

Concurrent Measurement of Deep-Inelastic Virtual Compton Scattering

R. Cester, C. M. Hoffman, F. C. Shoemaker, and M. Strovink*

Joseph Henry Laboratories, Princeton University, Princeton, New Jersey 08540

June 15, 1973

*Address after July 1, 1973: Physics Department and Lawrence Berkeley Laboratory, University of California, Berkeley, California 94720

ABSTRACT

While conducting our heavy neutral muon search, we plan to study deep-inelastic virtual Compton scattering, where the incident spacelike photon is radiated by a muon, and the outgoing timelike photon decays into two muons. This process is of fundamental importance as a probe of hadron structure by two photons. A recent experiment has yielded the intriguing result that Compton cross-sections at high momentum transfer appear to be much larger than even the parton-model estimates. This result can be checked in our experiment with improved statistics, and the study of the Compton process can be extended to a much wider range of kinematic variables.

INTRODUCTION

The strikingly large continuum electron-proton cross-sections observed at SLAC[1] have stimulated intense interest in the charge structure manifested by hadrons at large momentum transfer. In the familiar notation of Drell and Walecka,[2] the proton's inelastic structure function $\nu W_2(Q^2,\nu)$ appears to behave as a function only of the scale-invariant quotient of these variables. The absence of scale in the cross-section suggests, in turn, the existence of pointlike hadron constituents.

As speculations on these phenomena soar, it becomes essential to broaden the base of pertinent experimental work. With the advent of higher energies at NAL, the obvious extensions of inclusive-lepton-scattering measurements to higher Q^2 are proceeding apace, with variety in the type of probe (muon and neutrino) and in the type of group. We assume for the present that the combination of these efforts will yield a clear result. Equally naturally, one needs to investigate companion processes which are not the same as the reaction which parton and light-cone phenomenologies are designed to explain. Examples are the $pp \to \ell^+\ell^- X$ measurements of the Lederman group at BNL, ISR, and NAL. However, interpreting processes in which hadrons probe hadrons creates the need to assume mechanisms (e.g. annihilation) of parton-parton interaction. For the inelastic Compton reaction with which we are concerned, $\gamma_v N \to \gamma_v X$,

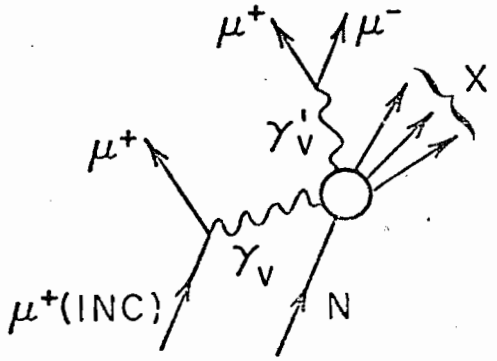

ability to restrict attention to the photon-hadron vertex and to sum over hadron states is preserved, while the kinematic variables can be brought into the deep-inelastic range. The nature of the photon-hadron interaction, however, is more complex here than for lepton inelastic scattering, which is dominated by the absorption of a single photon. For the Compton process in which a photon is scattered, two photons probe the hadron structure and bilocal effects can play an important role.

In 1969 Bjorken and Paschos,[3] using a simple parton model, computed a differential cross-section for inelastic Compton scattering of real photons which is simply related to that for inelastic lepton scattering. This computation was extended[4] to the case of a timelike final-state photon, decaying into muons. Brodsky and Roy[5] observed that the Bjorken-Paschos model enjoyed field-theoretic justification only for instantaneous two-photon interaction with partons, which may dominate only in a region of small energy transfer to hadrons. Comparison of theory and experiment outside this region could clarify the issue: does point-like constituent behavior occur whenever the momentum transfer is large, or must additional requirements be met? Lastly, Iliopoulos and Paschos[6] found a kinematic region of virtual Compton scattering to which light-cone ideas may apply, but which, unfortunately, appears to lie beyond near-term experimental reach.

Our interest in deep-inelastic Compton scattering has been intensified by a spectacular result obtained recently at Cornell.[7] Real photoproduction of low-mass muon pairs was measured for the first time in the scaling region, $t > 1.7\ (\mathrm{GeV}/c)^2$. Observed cross-sections exceeded the Bjorken-

Paschos prediction (and the Bethe-Heitler background) by one order of magnitude! That the Bjorken-Paschos model should not be confirmed perhaps is not surprising, in view of the theoretical uncertainties, and the possibility that photons, like hadrons, scatter almost exclusively at low t. That their parton model should underestimate the Compton cross-section by a factor of ten, on the other hand, is astounding, and must be investigated further.

Before our proposed measurement is discussed in more detail, other related experimental work should be mentioned. Elastic real Compton scattering has been measured at SLAC[8] up to $t = 1.1\ (GeV/c)^2$. We are not aware of a correspondingly unambiguous measurement of inelastic real Compton scattering. Prospective users[9] of the NAL electron-photon facility have proposed to look at deep-inelastic real Compton scattering above $t = 1\ (GeV/c)^2$. This kind of experiment in the past has been plagued by γ-ray background from π^o decay, which, in view of the recent ISR results,[10] may be more copious at large t than these proponents have assumed. Despite this background and the rate advantage of the experiment proposed here, we feel that the strongest argument in favor of measuring virtual Compton scattering is the ability to vary the mass of the virtual photons. In particular, the timelike photon mass can be fixed at values ($\sim$ 0.3 GeV) appropriate for the urgently needed check of the Cornell measurement, and can be swept to higher levels for further exploration.

EXPERIMENTAL TECHNIQUE

Virtual Compton scattering, with the final-state photon decaying into two muons, has a differential cross-section in the Bjorken-Paschos model which is smaller than that for inelastic lepton scattering by a factor somewhat less than α. In addition, if the incident virtual photons are radiated by muons, a Weiszacker-Williams factor of similiar magnitude further depresses the event rate. Since the virtual photon flux carried by a muon has Q^2 sharply peaked near the muon mass-squared, rate considerations demand that incident photons be used which are nearly real. At this point one may ask: Why not perform this experiment in a photon beam, rather than in a muon beam? The answer rests on the ability of energetic muons and their associated virtual photon flux to pass through an enormous target thickness without significant attenuation. The target for the Compton measurement proposed here is the same 30 ft of Fe which would be used in our neutral heavy muon search. While amounting to only 2% of a muon-radiation length, it has 1200X more nucleons/cm^2 than one electron-radiation length of liquid hydrogen. Integrating the Hand[11] flux of virtual photons

$$\frac{d^2\Gamma}{dQ^2 dk} \simeq \frac{\alpha}{2\pi Q^2} \frac{k}{E^2} \left\{ 1 - \frac{2\mu^2}{Q^2} + \frac{2E(E-k)}{k^2} \right\}$$

over Q^2 and an appropriate range of photon energy k, one obtains 4×10^{-3} photons with average energy 100 GeV, per 200-GeV muon. Folding in the ratio of target thicknesses mentioned above, a beam of 10^6 muons per pulse, incident on our spectrometer, becomes the equivalent of 5×10^6 tagged photons per pulse, of known variable mass and energy.

We plan to measure the virtual Compton process at the same time and using exactly the same apparatus with which we have proposed to search for heavy neutral muons. The Compton signature, one muon in and three muons out, is like that for muon tridents, with the important difference that significant energy is transferred to hadrons. The latter property insures that, unlike tridents, the Compton events can satisfy the same trigger requirement used for heavy neutral muons: at least two muons in the final state, with a measurable hadron shower. The energy and direction of the incident and three final muons are determined by the iron-magnet proportional-chamber spectrometer. Thereby, the energy and momentum transfer to hadrons are specified independent of assumptions concerning the relative contributions of various Feynman graphs. For the heavy neutral muon experiment, the calculated geometric detection efficiency averages 50%, with about half the inefficiency due each to spectrometer aperture and to soft-muon range. Since the Compton process generally involves smaller transverse momenta, the aperture effects are expected to be even less important. In calculation of backgrounds and rates, we have required that at least 25 GeV be transferred to hadrons, in order to satisfy trigger and background-suppression requirements. Also, the energy of the final-state muon pair has been required to exceed 25 GeV, in order to avoid inefficiency due to muon range. After these cuts are made, we expect the Compton detection efficiency to lie near unity.

BACKGROUNDS AND RATES

Backgrounds to the Compton amplitude are of importance in certain kinematic regions, which should be identified prior to discussion of event rates. Therefore, we consider backgrounds first.

The lowest-order diagrams giving rise to three muons in the final state, along with our notation, are reproduced in Fig. 1. The Compton graph is the only one which offers new information on hadron charge structure, since nuclear absorption of the single photon in the other graphs is described by the same structure functions measured in inelastic lepton scattering. In addition to the spacelike absorbed photon, these background diagrams have an internal photon and a muon propagator. We have attached the labels "Bethe-Heitler" and "bremsstrahlung" to the graphs having, respectively, spacelike and timelike internal photons. These graphs are the same as those giving rise to muon tridents, except that our insistence on large energy and momentum transfer to hadrons requires the nuclear form-factors to be evaluated for the continuum, rather than resonance, elastic, or coherent-nuclear regions. The total muon-trident cross-section is about 2×10^{-32} cm^2/nucleon in Fe at 200 GeV,[12] while cross-sections of interest here are smaller by $\sim$5 orders of magnitude. The necessary rejection of non-continuum background can be achieved as follows:

(1) Evidence of a hadron shower must be present both in the scintillation counters at time of triggering, and in the proportional-chambers at time of analysis. Such a shower could be simulated by multiple bremsstrahlung of the final-state muons (probability $\lesssim 10^{-4}$).

(2) The event reconstruction must show (typically) $t > 2$ (GeV/c)^2. Spectrometer resolution on projected transverse momentum of a single muon

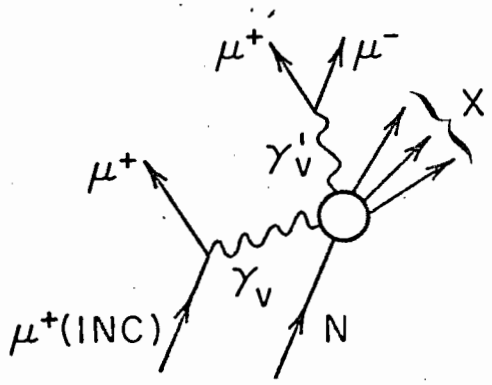

COMPTON

PARTICLE	4-MOMENTUM
μ^+(INC)	E
γ_v	k
γ_v'	k'
N	P

SCALARS: $k'^2 \equiv m^2$

$-(k-k')^2 \equiv t$

$2P\cdot(k-k') \equiv \nu$

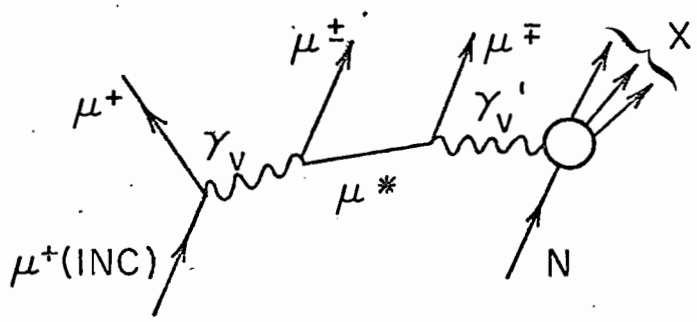

BETHE-HEITLER

PARTICLE	4-MOMENTUM
μ^+(INC)	E
γ_v	k
$\mu^\pm$	p_3
$\mu^\mp$	p_4
μ^*	p*
γ_v'	k'
N	P

SCALARS: $(p_3+p_4)^2 \equiv m^2$

$-k'^2 \equiv t$

$2P\cdot k' \equiv \nu$

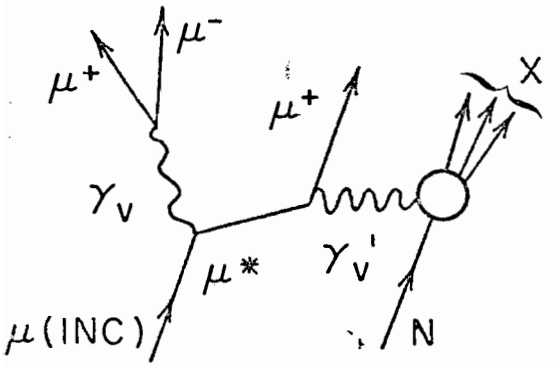

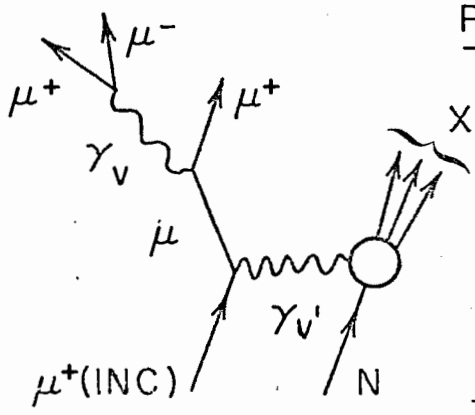

BREMSSTRAHLUNG

PARTICLE	4-MOMENTUM
μ(INC)	E
γ_v	k
γ_v'	k'
μ^*	p*
N	P

SCALARS: $k^2 \equiv m^2$

$-k'^2 \equiv t$

$2P\cdot k' \equiv \nu$

FIG. 1

is $\pm$150 MeV/c. For three muons carrying half the incident energy, this corresponds to a mean noise in t due to spectrometer resolution of 0.27 $(\text{GeV/c})^2$. Accordingly, the minimum t requirement appears defeatable only by an unusual fluctuation in precision of reconstruction, occurring with probability at most $\sim 10^{-2}$.

(3) Additional requirements on minimum and maximum combined energy of the final muons, and on concentration of events in kinematic regions favored by the continuum processes, should yield additional rejection of at least 1-2 factors of ten.

Therefore, rejection of non-continuum processes appears to be at least adequate.

Attention is turned to the problem of finding phase-space regions in which the Compton amplitude may be large relative to continuum Bethe-Heitler and bremsstrahlung amplitudes. The background graphs contain the same number of photon vertices, but one additional muon propagator. In these graphs, the propagator associated with the nuclear photon γ_v' is t^{-2}, which is small if we require large t. In the Compton graph, t may be large without forcing any propagator to become small. If $\vec{k}$ is nearly collinear with $\vec{E}$, the γ_v propagator in both the Compton and Bethe-Heitler graphs can be as large as $\sim \mu^{-2}$. Also, if $\vec{p}^*$ is nearly collinear with $\vec{E}$ in the Bethe-Heitler graph, the μ^* propagator in that diagram can be of the same order. In contrast, the γ_v and μ^* propagators in the bremsstrahlung graphs can each be no larger than $\sim m^{-2}$, where m is the mass of the muon pair. As a consequence, when m^4 is appreciably greater than μ^4, we expect the bremsstrahlung amplitude to contribute a far smaller background than does the Bethe-Heitler. At smallest m, the bremsstrahlung graph still

appears not to be a serious background, since it contains an extra lepton propagator, and a photon propagator which is necessarily small at large t.

In order to simplify the computations, we have assumed that the problem of separating Bethe-Heitler and Compton processes for slightly virtual incident photons is not much different than for real incident photons. The heuristic justification is that Q^2, peaked at $\sim \mu^2$, is small with respect to the other masses-squared (m^2,t) in the diagrams. Numerical computations have been performed of the cross-section differential in $\ell n(m^2)$, t, and ν for both processes with 100-GeV real photons incident. For the Compton process we have used the Bjorken-Paschos result. For the Bethe-Heitler process, we have used the Drell-Walecka cross-section[2] differential in the final muon vector momenta. In both cases a scale-invariant extrapolation has been made of nucleon structure functions measured at SLAC.[1] Transformation to a Bethe-Heitler cross-section differential in the desired variables was effected by numerically evaluating the Jacobian, and numerically integrating over remaining orientational variables. Finally, both differential cross-sections were numerically integrated over ν, between limits discussed in the previous section, and over t above a minimum value t_{min}. Since such computations are tedious and subject to inadvertent error, ours were checked by redundant efforts, inverse computations, and hand calculations where practical.

The resulting cross-sections $d\sigma/d(\ell n\ m^2)$ with $t > t_{min}$ are plotted vs. m^2, with t_{min} as parameter, for both processes in Fig. 2. It is seen that the Compton process is enhanced relative to the Bethe-Heitler at small m^2. This is a consequence of the fact that large m^2 makes the γ_v' propagator

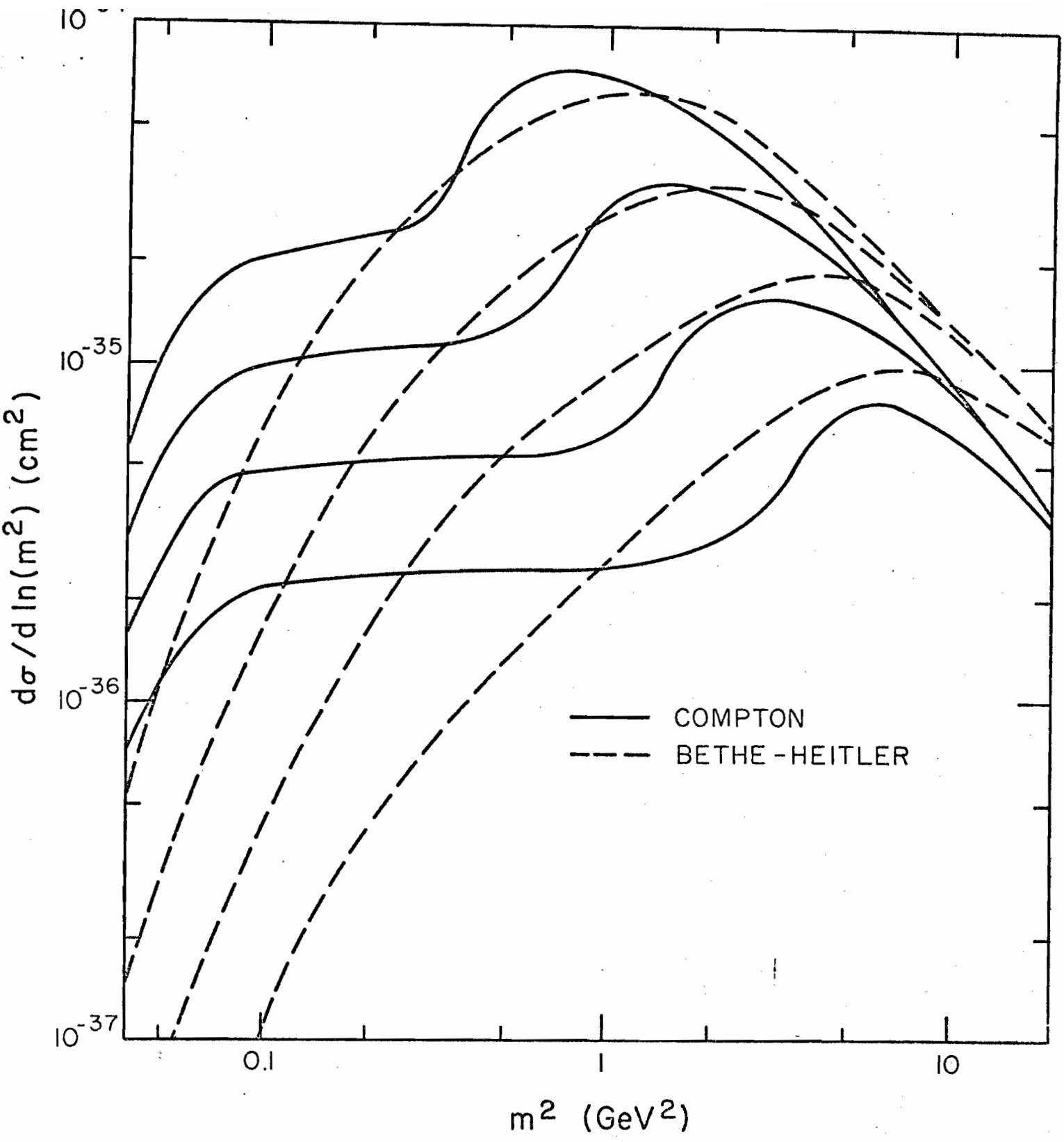

Figure 2

$d\sigma/d\ell n(m^2)$ vs. m^2 (muon pair mass-squared) for Compton scattering (Bjorken-Paschos parton model) and continuum Bethe-Heitler scattering of 100 GeV real photons on an average of proton and neutron target. The curves are computed for 4 minimum values of t (momentum-transfer-squared to hadrons): t_{min}= 1,2,4 and 8 $(GeV/c)^2$. Of course, the largest cross-sections correspond to the smallest t_{min}. The irregular quality of the Compton curves is caused by our restriction 25 GeV < (energy transfer to hadrons) < 75 GeV.

small in the Compton graph. For $m^2 = 0.1$ GeV^2 and $t > 2$ GeV, corresponding roughly to the Cornell experiment, the Bethe-Heitler cross-section is smaller than the Bjorken-Paschos Compton cross-section by a factor of 6. At larger m^2, the two cross-sections are of comparable size. Iliopoulos and Paschos have remarked that symmetric detection of the μ^+ and μ^- γ_v decay products, as would occur in our spectrometer, causes the Compton and Bethe-Heitler amplitudes to combine incoherently. If the bremsstrahlung diagrams can be neglected, as appears to be case for all but smallest m^2, there would be no need for periodic reversal of muon beam polarity to eliminate interference terms between Compton and background amplitudes.

Additional tricks may be useful in suppressing Bethe-Heitler background. Two have occurred to us. First, when $\vec{E}$, $\vec{k}$, and $\vec{p}^*$ are nearly collinear in the Bethe-Heitler diagram, as is the case when the γ_v and μ^* propagators are near maximum, one has the approximate relation

$$\frac{t}{m^2} = \frac{|\vec{k}|}{|\vec{p}_4|} - 1 \quad .$$

Second, believing for the moment the Bjorken-Paschos model for Compton scattering, one finds a large contribution to the cross-section when ν is near the maximum allowed value.[13] Cutting out the first small region of phase space, or all but the second, may further suppress considerably the background processes relative to the reaction of interest.

The cross-sections in Fig. 2 for 100-GeV photons incident were converted to event rates for 200-GeV muons incident, in the following way. First, the aforementioned Hand flux factor of .004 photons/muon was applied. This procedure is made plausible by the fact that it gives correct cross-

sections for inelastic lepton scattering, and that, for most of the photon flux, the departure from $Q^2 = 0$ is too small to affect the cross-section. Next, we have assumed that the number of events obtained using a photon spectrum of mean energy 100 GeV, is equal to that obtained using the same number of 100-GeV photons. Finally, we have multiplied by the sensitivity (4000 events/10^{-36} cm^2) of our experiment, which requires 10^{12} 200-GeV muons. With the previously mentioned restrictions on minimum energy transfer to hadrons and minimum muon pair energy, event rates computed in this way are believed to be corrected for the principal sources of triggering and detection inefficiency, but do not reflect allowance for contingencies.

The resulting event rates for deep-inelastic virtual Compton scattering and for Bethe-Heitler background are presented in Table 1, for various regions of t and m^2. In the bin roughly corresponding in these variables to the Cornell experiment, $t > 2$ and $.04 < m^2 < .2$, we expect 50 Bethe-Heitler and 220 Compton events in the Bjorken-Paschos model. The Cornell experimenters expected 15 Bethe-Heitler and 43 Compton events using the same model, but observed 630. Also by way of comparison, the Santa Cruz group, again using the Bjorken-Paschos model, have proposed[9] to collect 200 Compton events which may be relatively background-free, for $t > 1$ and $m^2 = 0$. Our corresponding sample would be 3200 Compton events with $t > 1$ and $.04 < m^2 < 20$, of which $\sim$ 500 would be relatively free of Bethe-Heitler background. If, as is indicated by the Cornell data, experimental Compton cross-sections are one order of magnitude higher than the Bjorken-Paschos results, our experiment could collect more than 1000 Compton events, with negligible Bethe-Heitler background, for $t > 8$ and $m^2 > 5$. In

TABLE 1

	$.04 < m^2 < .2$ $(GeV/c^2)^2$	$.2 < m^2 < 1$	$1 < m^2 < 5$	$5 < m^2 < 20$
$t > 1$ $(GeV/c)^2$	460 (180)	1330 (1090)	1190 (1300)	230 (320)
$t > 2$	220 (50)	390 (400)	760 (790)	220 (310)
$t > 4$	110 (15)	140 (130)	330 (380)	200 (280)
$t > 8$	50 (3)	65 (35)	100 (130)	135 (190)

Anticipated number of deep-inelastic virtual Compton events, per 10^{12} 200 GeV muons, calculated according to the Bjorken-Paschos parton model. The numbers in parentheses are Bethe-Heitler background. The expected event sample has been divided into ranges in t (momentum-transfer-squared to hadrons) and in m^2 (mass-squared of the muon pair). Only events with muon pair energy > 25 GeV and energy transfer to hadrons > 25 GeV have been included. A recent Cornell experiment indicates that the Compton rate may be higher than calculated here by at least one order of magnitude.

any case, the need for additional experimental work in this area is urgent, and the experimental procedure clear: any measured departure from the fully calculable rates for one-photon processes, which survives the necessary scrutiny, can be interpreted as arising from the Compton diagram.

REFERENCES

(1) G. Miller et al., Phys. Rev. D5, 528 (1972), and references cited therein.

(2) S. D. Drell and J. D. Walecka, Ann. Phys. 28, 18 (1964).

(3) J. D. Bjorken and E. A. Paschos, Phys. Rev. 185, 1975 (1969).

(4) J. D. Bjorken and E. A. Paschos, Phys. Rev. D1, 1450 (1970).

(5) S. J. Brodsky and P. Roy, Phys. Rev. D3, 2914 (1971).

(6) J. Iliopoulos and E. A. Paschos, Phys. Rev. D6, 1340 (1972).

(7) J. F. Davis et al., Phys. Rev. Letters 29, 1356 (1972).

(8) R. L. Anderson et al., Phys. Rev. Letters 25, 1218 (1970).

(9) C. A. Heusch et al., NAL Proposal 152, Addendum II (1972).

(10) L. Lederman et al., to be published.

(11) L. Hand, Phys. Rev. 129, 1834 (1963).

(12) M. J. Tannenbaum, NAL Summer Study Report B.2-68-32, 1968.

(13) The steep functional dependence of the Compton cross-section on ν also favors the emission of low energy dimuons, thereby reducing to a minimum the ambiguity in $\mu^+\mu^-$ pairing.

Addendum 203

Correspondent: M. Strovink
FTS/COM 415-843-2740 Ext. 5501

EXPLORATION OF RARE MUON-INDUCED PROCESSES

(ADDENDUM II TO FERMILAB PROPOSAL 203)

A. R. Clark, E. S. Groves, L. T. Kerth,
S. C. Loken, M. Strovink, W. A. Wenzel

Department of Physics and
Lawrence Berkeley Laboratory,
University of California, Berkeley, CA 94720

and

R. Cester, F.C. Shoemaker, P. Surko, M.S. Witherell

Joseph Henry Laboratories,
Princeton University, Princeton, N. J. 08540

and

R. P. Johnson
Fermi National Accelerator Laboratory
Batavia, Ill. 60510

February 18, 1975

I. INTRODUCTION

Now that the Fermilab muon beam has exceeded design intensity and provided significant illuminations to both first-stage muon scattering experiments, the program requires experimental apparatus which would realize a broader range of muon physics objectives. High acceptance over the full length of a distributed iron target-spectrometer can provide the necessary sensitivity to rare processes. Nearly continuous iron can suppress $\pi \to \mu\nu$ decay background and provide the medium for calorimetric determination of energy transfer to hadrons. Fast detectors can tolerate further increases in beam intensity while maintaining acceptance for multiple final-state muons even within the beam area.

We first proposed to build such a spectrometer two years ago. The purpose of this Addendum is to consolidate the experimental groups who would participate in the experiment, to present further information on its design and implementation, and to update our physics objectives. In addition, we describe the capabilities of the experiment which have direct relevance to recent discoveries of new particles[1] and evidence of direct muon production[2]. The first two topics are addressed in section II and the Appendices; the initial experimental objectives are enumerated below and described in greater detail in part III. Longer-range plans are described in part IV.

The initial physics objectives are mutually compatible. They are:

(1) Search for heavy neutral muons predicted by gauge theories in the mass range 2 - 10 GeV, and other new particles decaying into one muon. The sensitivity for analyzed events is $1 - 2 \times 10^9$ events/μb.

(2) Measurement of deep-inelastic virtual Compton scattering and search for other deep-inelastic $\mu^+\mu^-$ pair creation.

(3) Measurement of the deep-inelastic muon scattering structure function at very high momentum transfers. For example, 8200 events exceeding $Q^2 = 160$ $(GeV/c)^2$ will be obtained.

(4) Collection of $2 - 3 \times 10^4$ $\psi \rightarrow \mu^+\mu^-$ decays and data at higher dimuon masses. The $\psi\mu\mu$ coupling will be measured in the range -15 $(GeV/c)^2 < q^2 < 0$ with 7% statistics at $q^2 = -m_\psi^2$.

II. THE SPECTROMETER

The design of the magnetized iron spectrometer, shown in Figure 1, is substantially the same as that described in the original proposal. We will discuss here only those features which have changed.

The total length of iron in the spectrometer has been decreased from 50 ft to 30 ft, and the cross-section of the active area has been increased to 3.5 x 6 ft (from 3 x 4 ft). These changes reduce the tonnage of iron by 31% from the original proposal. Compensating improvements in acceptance and in detector information will minimize the effect of this change on the yield of events passing final cuts. The decreased length makes possible a finer granularity in the detector system, giving more and higher quality information for each event.

The details of one module of the spectrometer are shown in Figure 2. The apparatus consists of 18 such units. Each module consists of 5 magnetized iron plates, 4 inches thick. Between each plate is a calorimeter counter similar to those described in Proposal 307, Appendix C. These provide a measurement of the hadron energy with accuracy $\sigma(E) \approx 0.9\,E^{\frac{1}{2}}$. In addition, the calorimeter counters locate the interaction vertex for "noisy" events and are used in the trigger logic to detect showers and to veto unscattered muons. Three independent triggers, using the same counter hodoscopes, will be used in parallel. A thorough discussion of trigger efficiencies and rates appears in Appendix 4.

At the downstream end of each module there is a fifth calorimeter counter and a proportional counter-drift chamber system to locate precisely secondary muon tracks as well as the incident track upstream of the interaction. Alternate banks also contain a trigger hodoscope for the single and multiple muon triggers. An exploded view of the trigger-detector system is shown in Figure 3.

The use of proportional chambers, as originally proposed, provides the good time resolution and multitrack efficiency necessary to take data at instantaneous beam fluxes up to 10^7/ sec. We have added a drift chamber to each detector to achieve high spatial resolution in the bending plane. This results in a significant improvement in momentum resolution, which ranges from 7% to 11%.

The engineering group at LBL has made an independent conservative cost estimate of the muon spectrometer. This study (Appendix 1) indicates that the total cost of the magnet will be less than $240 K. The cost of instrumentation (Appendix 2) is less than $210 K.

The time scale for construction, assuming approval is received at the March meeting of the PAC, is shown in Fig. 5. Installation of the spectrometer can begin in February 1976. The critical path is determined by the delivery time for the steel. An informal quote from a supplier is 5 months. If distressed steel is available, the time scale can be accelerated by several months.

As indicated in Appendix 3, the responsibility for the construction and installation of the apparatus will be shared by all of the collaborators. There are 11 Ph.D. physicists for whom this experiment will be the major research commitment. We will have 5.5 FTE Ph.D.'s, 2 FTE technicians, at at least 2 FTE graduate students in residence at Fermilab during the installation and operation phases of the experiment.

The spectrometer will be oriented with its magnetic field vertical. This allows data to be taken concurrently with operation of the Chicago Cyclotron Magnet upstream, bending the beam toward the East. This assumes that at beam energies less than the maximum, the CCM field is scaled accordingly, as has been the practice of the E98 group [3]. The spectrometer will be placed so that the beam is centered in the spectrometer with the CCM on. If the CCM is off, the beam can also be centered using magnets in Enclosure 104.

In addition to data-taking, we require test running at lower muon beam energy for calibration of the magnetic field in the spectrometer. We also need test runs with a hadron beam at several energies for calibration of the calorimeter and measurement of hadron punch-through probabilities.

III. DISCUSSION OF EXPERIMENTAL OBJECTIVES AND TECHNIQUE

A. Search for heavy neutral muons predicted by gauge theories, and for new particles giving rise to a two-muon final state.

A discussion of the theoretical motivation for searching for $\overline{M}^{o}$'s and a close examination of their possible experimental properties are contained in the original proposal. Briefly, the $\overline{M}^{o}$'s could be produced by deep-inelastic interactions of μ^{+}'s with nucleons via W^{+} exchange, and would quickly decay to $\mu^{+}\mu^{-}\bar{\nu}_{\mu}$ (B.R. $\approx$ 25%). The signature is one muon in, two out. The discovery of weak neutral currents [4] increases confidence in the Weinberg-Salam model (which contains no $\overline{M}^{o}$). At the same time, it imparts greater urgency to experiments which can test other predictions of gauge theories. For example, theories (III) and (V) catalogued by Bjorken and Llewellyn Smith[5] include neutral currents, require no M^{+} coupled to neutrinos (in agreement with experiment [6]) and also predict the existence of $\overline{M}^{o}$'s.

The trigger for $\overline{M}^{o}$'s and other inelastic multimuon processes is conceptually the same as that originally described. A coincidence is formed between a hadron shower signal from calorimeter counters upstream, and evidence of two muons in hodoscopes downstream of the shower. A quantitative description of the trigger and background rejection appears in Appendix 4. The trigger rate, dominated by inelastic scattering at low Q^{2} of one

muon in coincidence with an unvetoed muon in the same RF bucket, is less than 2×10^{-6} (per incident muon) at 10 MHz instantaneous rate.

The number of triggered and analyzed $\bar{M}^{o}$'s, using the same cross-section and branching ratio assumptions as on p. 19 of the original proposal, is:

M^o mass	Events/10^{12} muons
2 GeV/c^2	466
4	445
10	121

To suppress background from $\pi^- \to \mu^- \bar{\nu}_\mu$ decay, the original proposal described a set of kinematic cuts which removed about 1/2 of the signal as well. We expect that the higher density of information in the current version of the spectrometer will make such severe cuts unncessary. For example, the better calorimeter will allow us to reconstruct and cut on the missing (neutrino) energy.

It is important to emphasize the general nature of the particle search we will conduct. Apparent muon nonconservation can result from the weak decay of any new particle whose stronger decays are suppressed by old or new selection rules. Accordingly the capabilities of this experiment are restated in more general terms. With 225 GeV muons incident on Fe, the integrated luminosity is 3×10^{39} cm^{-2}. For example, this corresponds to 10^8 deep-inelastic muon interactions with $\nu > 50$ and $Q^2 > 2$. Compared to ordinary hadron reactions, each of these interactions is unusually violent, representing a prime source of new particle production. The excellent acceptance and trigger efficiency of the proposed spectrometer make it possible to detect most of the subset of these 10^8 interactions which contain one or more "directly produced" muons with energy $\gtrsim$ 20 GeV, in addition to the scattered muon. These are identified with high efficiency and reconstructed with negligible kinematic bias. The principal backgrounds are (1) $\pi \to \mu\nu$ decay, occurring at the 10^{-4} level,

and (2) inelastic μ tridents with one muon undetected. The identification and subtraction of these backgrounds is discussed in detail in the original proposal.

B. Measurement of Deep-Inelastic Virtual Compton Scattering

Since we discussed this measurement in Addendum I, new results from the U.C. Santa Barbara [7] and Rochester [8] groups have confirmed the anomaly originally observed at Cornell[9]: Inelastic processes involving two hadronic photons occur at rates typically one order of magnitude in excess of the parton-model predictions. Almost no related information exists in the much larger kinematic range accessible to this experiment at the Fermilab.

The trigger for Compton scattering is the same as for the $\overline{M}^{O}$ search. Evolution of the spectrometer design (part II) produces rate estimates approximately 70% of those in Addendum I, with considerably improved information on the final state.

Again, we emphasize that the virtual Compton scattering process [γ_v (spacelike) N → γ_v (timelike) X ; γ_v (timelike) → $\mu^+\mu^-$] is just one member of a general class of possible mechanisms for inelastic production of dimuons. For example, the timelike photon may be replaced by conventional or unconventional vector mesons. Detection of diffractive rather than deep-inelastic virtual photoproduction of massive dimuon states is discussed in some detail in a separate section (part D).

C. Deep Inelastic Muon Scattering

The spectrometer is well suited to a study of deep inelastic muon scattering, especially the behavior of the structure function νW_2 as a function of Q^2 and ν in the region $Q^2 > 150$ $(GeV/c)^2$.

The trigger has been designed to favor the high-Q^2 region by requiring an appreciable scattering displacement in the non-

bending (vertical) direction. Referring to Figs. 1 and 3, the trigger will require one or more counts from each of any two successive hodoscope banks, with no count in either of the associated beam-veto counters. In order to avoid biases in detection efficiency dependent on hadron energy, the trigger does not require a detected hadronic shower. Monte Carlo simulations give a total rate for this trigger of 2.6×10^{-6} triggers/incident muon, of which more than 80% are from real events. We have made conservative estimates of the background rates; the calculations are described in Appendix 4. None of the backgrounds presents a problem.

The reconstructed events will be characterized by $\sigma(1/E')$ between 7 and 11%. Coulomb scattering contributes 100-150 MeV/c uncertainty to the transverse momentum in the nonbending plane. The expected yield of triggered and analyzed events vs. Q^2 for 10^{12} muons at 225 GeV is shown in the table below:

Q^2 $(GeV/c)^2$	Events above this Q^2	Q^2 $(GeV/c)^2$	Events above this Q^2
40	7.8×10^5	160	8.2×10^3
60	3.6×10^5	180	3.3×10^3
80	1.7×10^5	200	1.3×10^3
100	8.8×10^4	220	450
120	4.1×10^4	240	152
140	1.9×10^4	260	48

D. Exploration of The Properties of ψ, ψ', and Other Massive Dimuon States

A quantitative calculation of ψ yields has been carried out. For conservatism, only transverse virtual photons having the usual ρ muoproduction flux and diffractive scattering from Fe were considered. Exact kinematics were used for Q^2_{min}, t_{min}, and t_{max} effects, with all masses finite. The E87 dimuon cross-section of .24 nb/Be nucleus at $Q^2 = 0$, $\nu = 150$ was used for all ν[11],

together with t_{min} restrictions on phase space. The cross-section and t slope parameter for Fe were scaled by $A^{2/3}$ from the Be values [10]. A ψ propagator = $1/(1 + Q^2/m_\psi{}^2)^2$ was used. For 225 GeV muons incident, the following cross-sections were obtained for ψ-like dimuon states. In each case we assume the same form for the propagator and the same value for the photon coupling constant.

Mass	$\sigma\mu\mu$ per Nucleon	Assumed $\mu\mu$ B. R. Relative to ψ	Effective $\sigma\mu\mu$ per Nucleon	$\mu\mu$ Decays in Target Total	$\mu\mu$ Decays in Target with 3 μ's penetrating 7 modules
(ψ) 3.1	11 pb.	1	11 pb	3×10^4	2×10^4
(ψ') 3.7	4	0.1	.4	1×10^3	700
6	.2	0.1	.02	50	35
9	.005	0.1	5×10^{-4}	1.3	1

The Q^2 - ν distribution of ψ's is shown in Fig. 6. The total number of $\psi \rightarrow \mu\mu$ decays occurring in the spectrometer target is 3×10^4, with $\sim$100 having $Q^2 > 10$.

Because of t_{min} effects, the calculated cross-sections are lower than one might naively expect. Even with the exceptionally high luminosity and acceptance in the proposed spectrometer, this method of search for higher mass ψ-like objects is limited. Higher energy muons would of course help, but e^+e^- rings (also of higher energies) would seem to be the best way of studying higher mass states.

Figure 6 illustrates two unique capabilities of this ψ experiment. The large sample ($2 - 3 \times 10^4$) of collected events permit a definitive (1%) measurement of g_A/g_V in $\psi\mu\mu$ coupling, if the beam helicity can be alternated. Unfortunately, this is a future development. Of immediate interest is the ψ production

rate at high $|q^2|$: a bin with median $q^2 = -m_\psi^2$ has $\approx$ 300 events. The q^2-dependence of the $\psi\mu\mu$ coupling (presumably ψ-γ coupling) therefore is measurable for $-15 < q^2 < 0$ as well as for $q^2 = 0$ (E87) and $q^2 = 9.6$ (SPEAR). A dramatic q^2-dependence of the type proposed in the "color" scheme of Bars and Peccei [12] would be easily detected.

A trigger for diffractive ψ production should not require the scattered muon either to be soft or to emerge at small angles. The former restriction removes most of the sample (cf. Fig. 6) and the latter deletes the high $-Q^2$ events. A promising trigger concept designed to suppress μ trident background is described in Appendix 4. The calculations required to specify the trigger acceptance and rate are not yet complete.

The ψ dimuons will be detected with chamber acceptance averaging 64% and mass resolution ranging from 6% in the best case to 10% for topologies with "minimal" information. The chief analysis background is expected to be incoherent muon tridents at the same low level as in E 87.

IV. FUTURE PLANS

The detector proposed here is well suited to the study of additional new physics when parameters of the Fermilab muon beam are extended. The most obvious parameter is muon energy. Weak interaction effects generally increase with energy, and the gain is especially dramatic when kinematic thresholds are involved. The dependence of M^o production on M^o mass and muon energy is discussed in the original Proposal 203. The deep-inelastic scattering data also will benefit from higher energy. In the proposed run, for example, raising E_μ from 225 to 300 GeV would increase the number of events with $Q^2 > 260$ $(GeV/c)^2$ from 50 to 1000. For diffractive muoproduction of vector particles (e.g., ψ's) the gain with increasing energy is dramatic, especially for exploration of higher mass states. Both t_{min} and threshold effects contribute to the improvement.

Control of muon helicity is a development with equally attractive possibilities for new measurements, particularly in the study of weak neutral currents. The implications for the muon-nucleon scattering cross-sections have been studied by Berman and Primack [13], Derman [14] and Suzuki [15]. Both the charge and helicity asymmetries increase as Q^2 and are of the order of a few percent at $Q^2 = 100$ (GeV/c)^2. The spectrometer we have proposed is particularly well suited to these measurements because of its high luminosity and acceptance, and symmetric detection of μ^+ and μ^-.

Another interesting problem is the search for an axial vector coupling in the muoproduction of ψ's. Present experimental limits on an axial component of the $\psi\mu\mu$ coupling are very weak. From $e^+e^- \to \mu^+\mu^-$ asymmetry measurements, we know only that $(g_A/g_v)^2 < 0.1$. In a broad view, such an interaction may be characterized without making specific assumptions about the Q^2 dependence of propagators and form factors. We emphasize that for $g_A/g_v << 1$, the search for g_A is better carried out with helicity rather than charge asymmetry measurements, because the former vary linearly with g_A/g_v, while the latter vary quadratically. In a comparison of cross-sections with well defined muon helicities at the presently proposed luminosity, the limit that can be set is in the range $g_A/g_v \lesssim 10^{-2}$, corresponding to a limit on the muon charge asymmetry in ψ-decay at the level of 10^{-4}!

Improvements to the muon beam of the types considered above in part can be made by increasing the accelerator energy. Continued improvements to the muon beam and its parent hadron beam are also needed. In particular, we note that **1)** the momentum range of the muon beam channel and its intensity can be increased without significant cost by the use of iron-focusing elements. **2)** the range and selectivity of the parent hadron beam should also be improved to increase the muon intensity at high momentum and to provide for the control of muon helicity.

Members of this group will continue their participation in the development of reasonable plans for effecting these essential improvements.

REFERENCES

1. J. J. Aubert et al., Phys. Rev. Lett. 33, 1404 (1974)
   J. E. Augustin et al., Phys. Rev. Lett. 33, 1406 (1974)
   C. Bacci et al., Phys. Rev. Lett. 33, 1408 (1974)
   G. Abrams et al., Phys. Rev. Lett. 33 1453 (1974).

2. J. P. Boymond et al., Phys. Rev. Lett. 33, 112 (1974)
   A. Benvenuti et al., Harvard, Pennsylvania, Wisconsin, Fermilab Preprint to be published.

3. T. B. W. Kirk, private communication.

4. F. J. Hasert et al., Phys. Lett. 46B, 138 (1973).

5. J. D. Bjorken and C. H. Llewellyn Smith, Phys. Rev. D7, 887 (1973).

6. B. C. Barish et al., Phys. Rev. Lett. 32, 1387 (1974).

7. D. O. Caldwell et al., Phys. Rev. Lett. 33, 868 (1974).

8. A. Melissinos, private communication.

9. J. F. Davis et al., Phys. Rev. Lett. 29, 1356 (1972)

10. The Fe (form factor)^2 was taken to be exp(-135 t).

11. NOTE ADDED IN PROOF: We have recently learned that the E 87 photoproduction cross-section is 16 nb, rather than 24 nb. All of our rates for Ψ production should be revised downward accordingly.

12. I. Bars and R. D. Peccei, "The Colorful ψ's", Stanford University Theoretical Reprint ITP-480, December, 1974.

13. S. M. Berman and J. R. Primack, "Weak Neutral Currents in Electron and Muon Scattering," SLAC Preprint, SLAC-PUB-1360 (TIE), December, 1973.

14. E. Derman, Phys. Rev. D7, 2755 (1973).

15. M. Suzuki, Nuc. Phys. B70, 154 (1974).

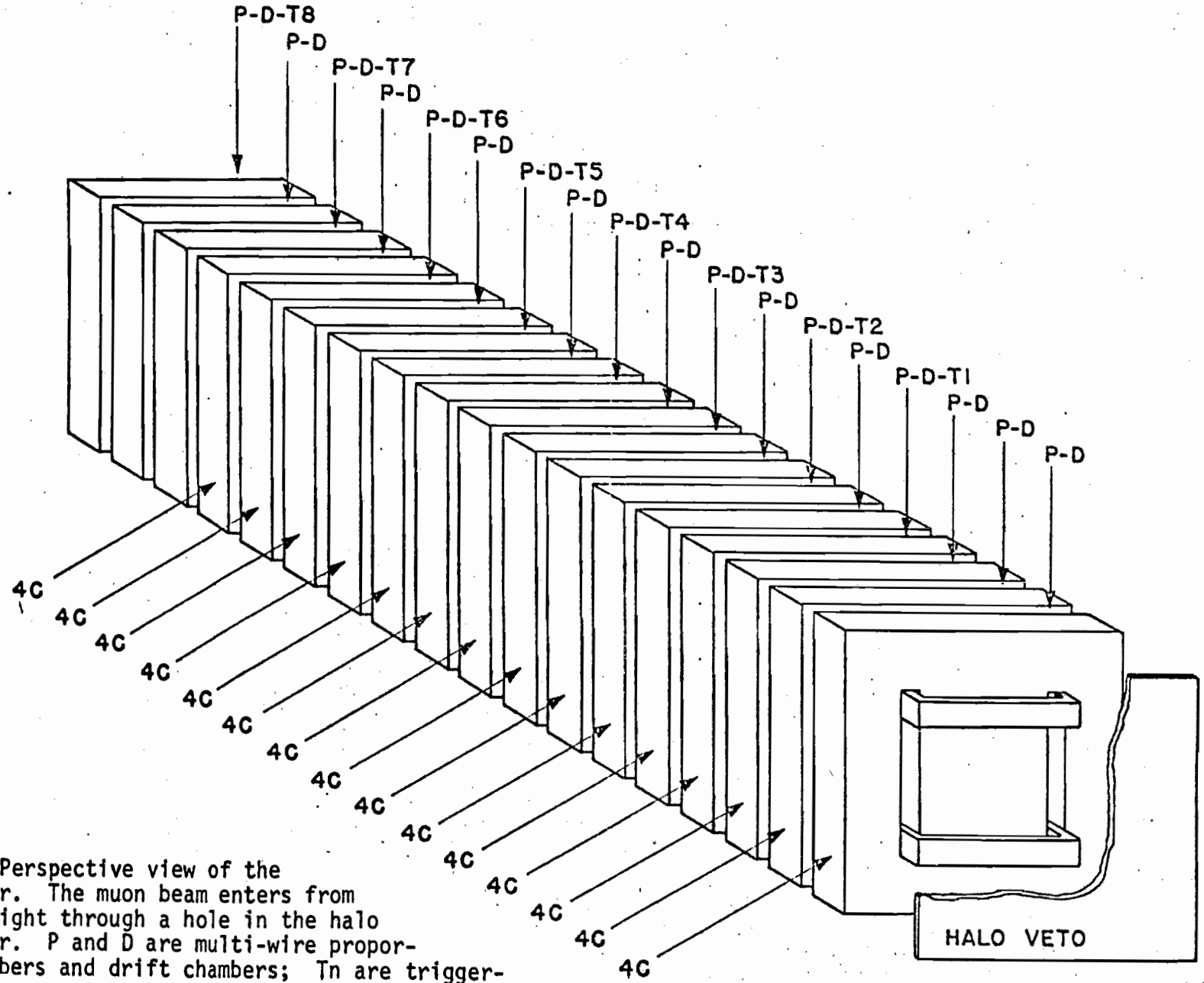

FIGURE 1. Perspective view of the spectrometer. The muon beam enters from the lower-right through a hole in the halo veto counter. P and D are multi-wire proportional chambers and drift chambers; Tn are trigger-hodoscope arrays with a beam veto/calorimeter counter. 4C indicates the four calorimeter counters within each magnet module. Also see Fig. 2 - 4.

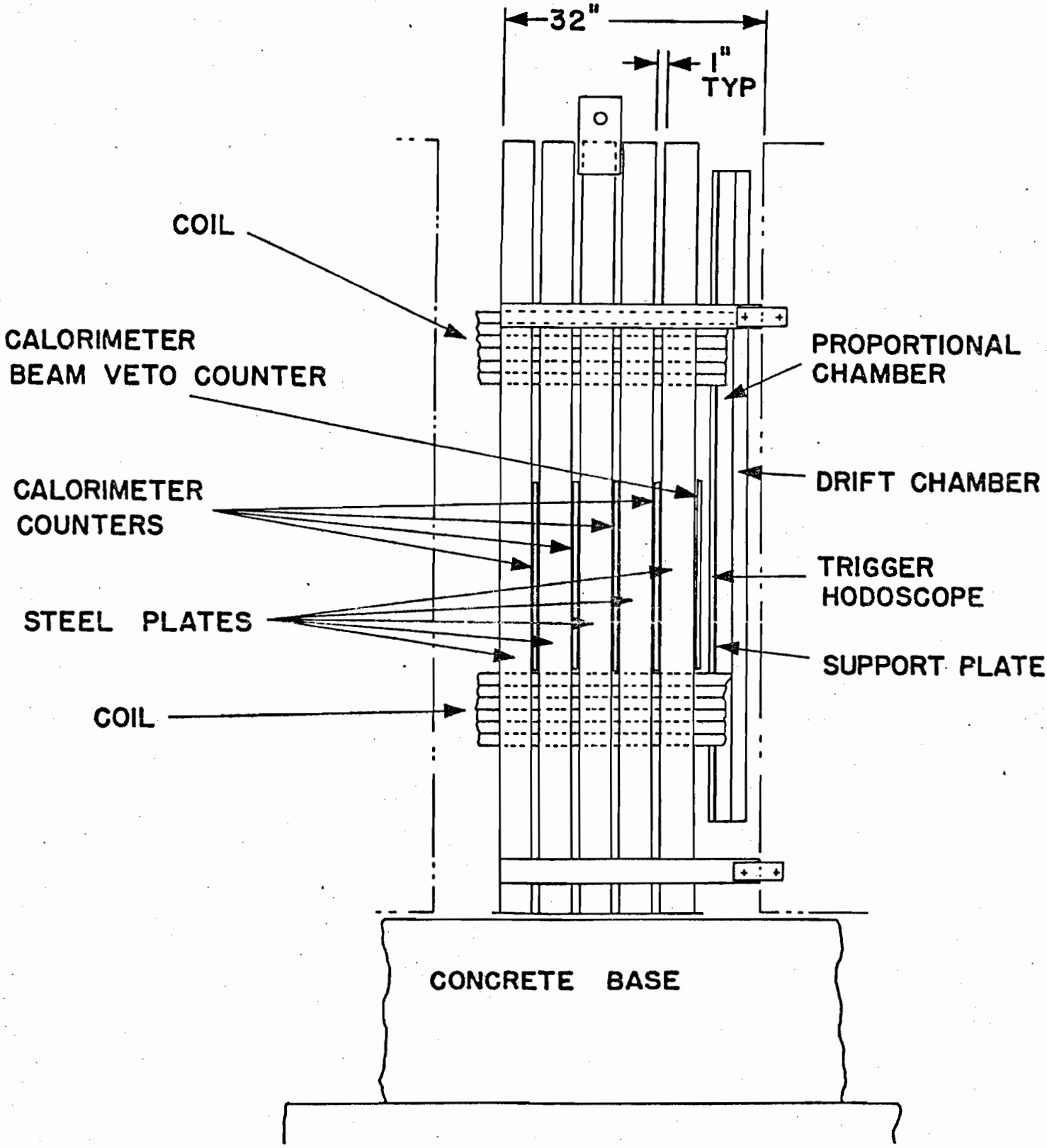

FIGURE 2. Elevation view showing detail of one module. The spectrometer consists of 18 of these modules.

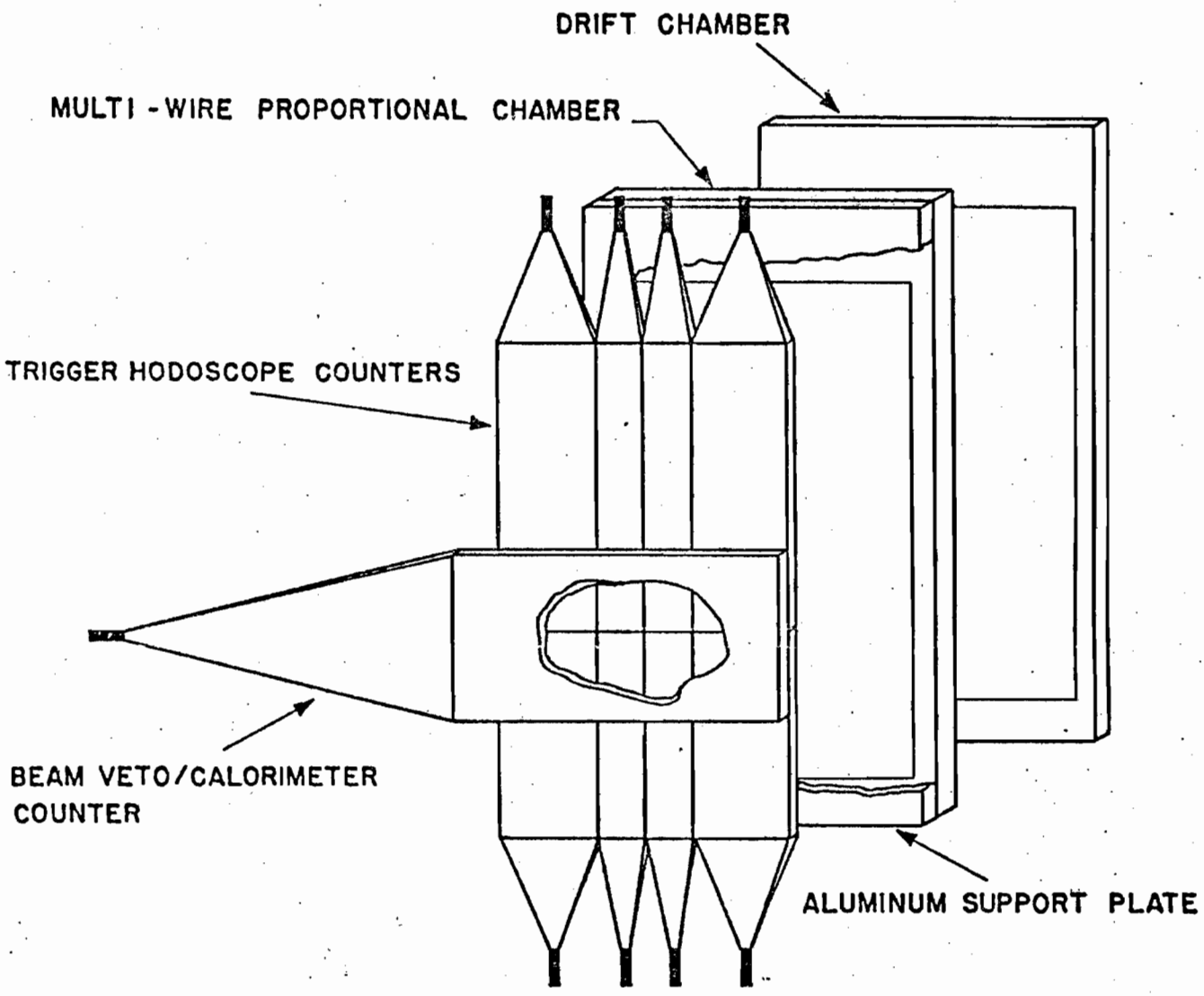

FIGURE 3. Exploded view of one trigger-detector assembly. All components are mounted on a single support plate to maintain alignment.

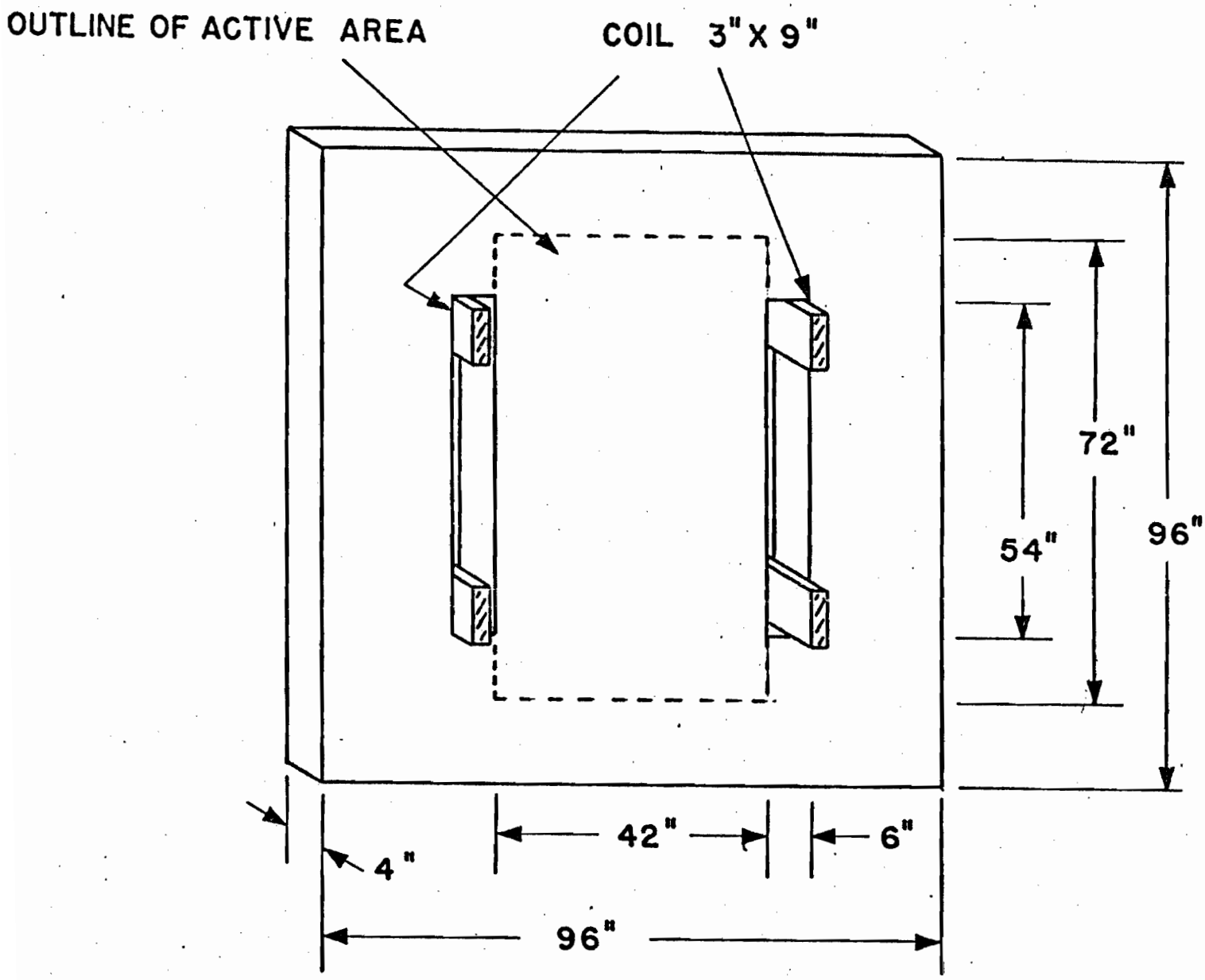

FIGURE 4. Magnet plate, detail.

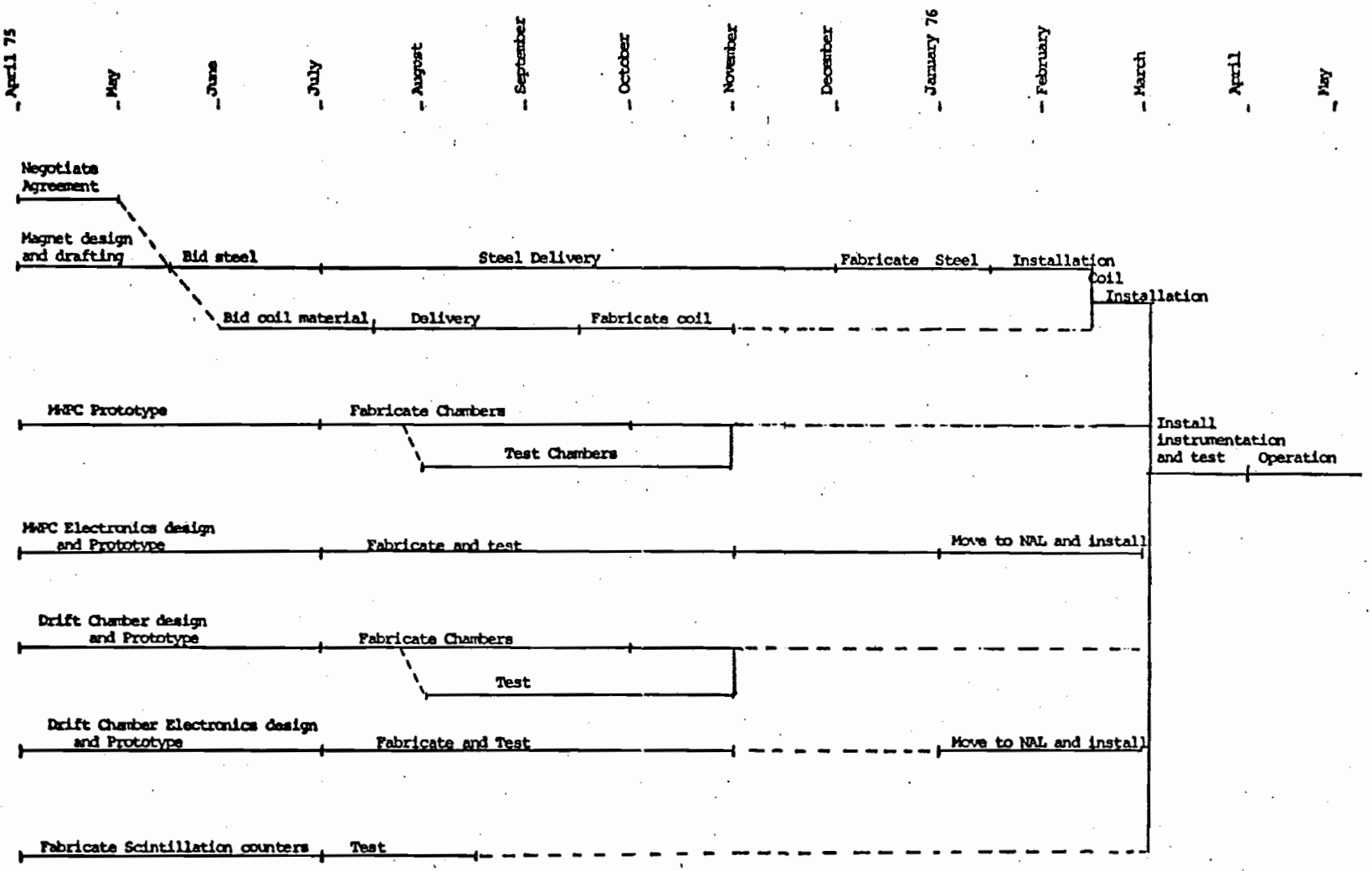

FIGURE 5. Design and fabrication schedule.

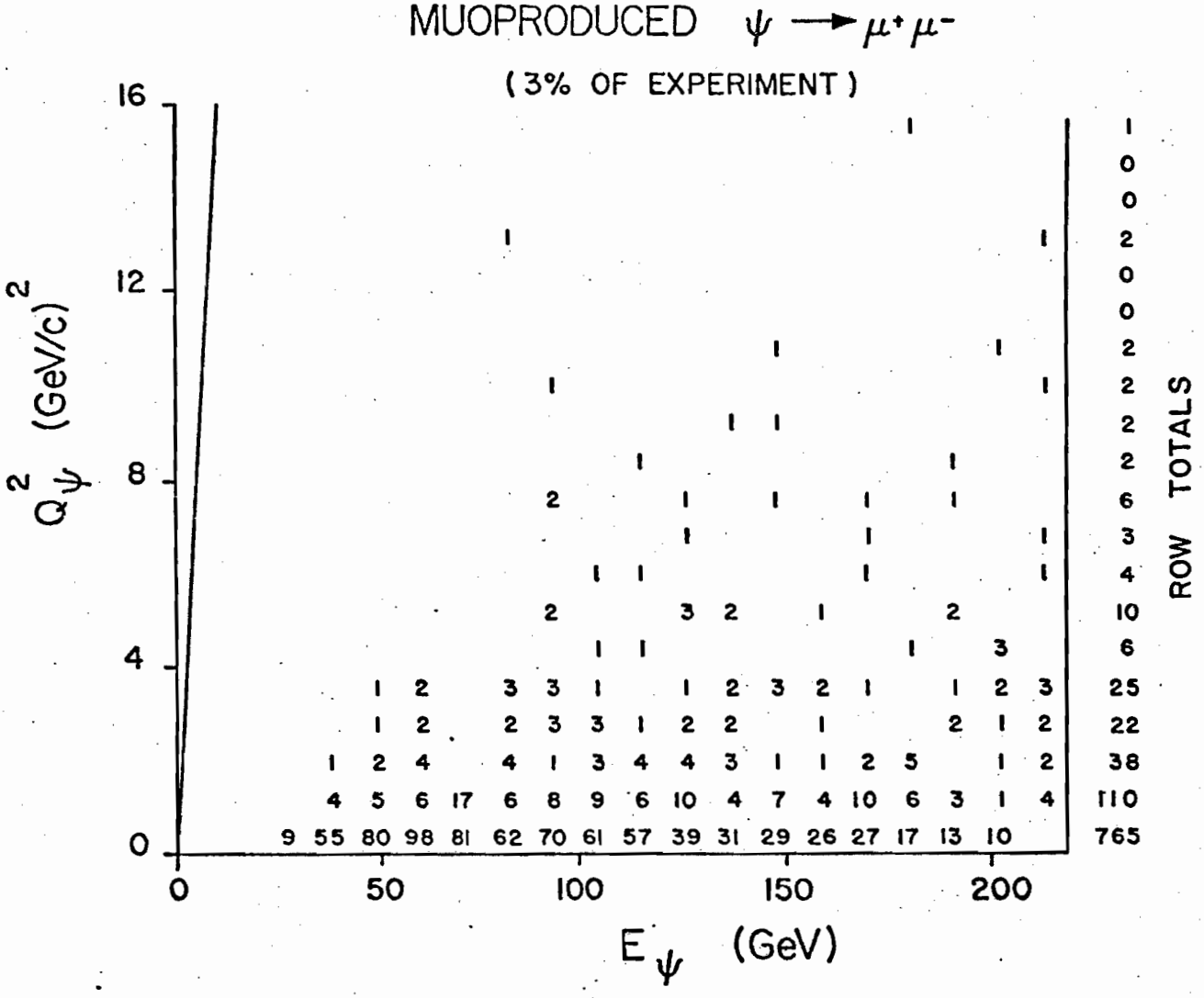

FIGURE 6: The Q^2 - ν ($\nu \approx E_\psi$) distribution of muoproduced ψ particles. The assumptions used in the Monte Carlo calculation are described in the text.

APPENDIX 1: MAGNET COST ESTIMATES

LAWRENCE RADIATION LABORATORY — UNIVERSITY OF CALIFORNIA

ENGINEERING NOTE

CODE	SERIAL	PAGE
AA0103	M4782 C	1 of 3

AUTHOR	DEPARTMENT	LOCATION	DATE
J. Gunn	Mechanical Engineering	Berkeley	December 2, 1974

PROGRAM — PROJECT — JOB

MECHANICAL ENGINEERING

COSTS, TIME STUDIES, ESTIMATING

TITLE

SECOND PARTIAL COST ESTIMATE FOR NAL EXP. P203

"A" Rev. 12/3/74 - DFR
"B" Rev. 2/7/75 - DFR
"C" Rev. 2/14/75 - DFR

This cost estimate covers only the iron-target iron magnet assembly, as discussed with A. R. Clark on January 28, 1975 for NAL Experiment P203. First proposal is on EN M4782. See UCLBL Dwg. 17L1934 for magnet module.

MAGNET STEEL PLATES - AISI 1020

Informal quote - Lukens Steel Company, Coatsville, Pennsylvania
17.8¢/lb, 5 month delivery (subject to escalation)
Estimated freight to Chicago: 2¢/lb

90 plates @ 10,633 lb/plate x 19.8¢/lb $189,480

MAGNET MODULE ASSEMBLY (18) COSTS

Labor to flame cut 180 holes (6" x 54" each) for coils and inserts: 367 hr @ $15/hr	5,505
Press insert into holes of each plate: 90 hr @ $15/hr	1,350
Weld up module: 244 hr @ $15/hr	3,660
Lifting beam for module assembly	500
Estimated freight Chicago to NAL @ 1¢/lb	9,569
	$ 20,584

ALUMINUM CONDUCTORS

Extruded alloy 1060F - 61% AICS conductivity
1.165 x 0.92 with 0.6 diam. hole x 60 ft straight section
Weight/ft = 0.954#
42 turns @ 120 ft/turn = 5,040 ft
Add 10% for spoilage ≃ 480
5,520 ft (5,266 #)

Quote from New Jersey Aluminum Company, Elizabeth, N.J.

Tooling charge:	$450	
Setup charge:	140	$ 590
Plus $1.035/lb x 5,266 lb		5,450
Plus estimated shipping to NAL @ 3¢/lb		158
	Conductor cost:	$ 6,198

COIL FABRICATION

Aluminum hose barbs	
4/turn x 42 turns = 168 required @ $1.05 ea	$ 176
Labor to weld to conductors	
C'bore: 56 hrs	
Weld: 56 hrs	
112 hrs @ $15/hr	1,680
Wrap conductors with heat shrinkable PVC tubing	
Material costs (9 rolls)	540
Installation 120 hr @ $15/hr	1,800
Thermal switches	
4 required @ $35 ea (installed)	140
Flow Switches	
1 required @ $200 ea (installed)	200
Hoses - 84 required @ 1.5 ft long @ 50¢/ft	63
Plus 84 hose clamps @ 75¢ ea	63
Plus installation: 32 hr @ $15/hr	480
Large supply hoses: 80 ft @ $2/ft	160
Manifolds - 2 required	
Materials	100
Labor: 30 hr @ $15/hr	450
Coil fabrication cost:	$ 5,852

MAGNET ASSEMBLY COSTS

Stack steel module:	100 man-hours	
Install coil:	80 "	
Pressure and flow check	20 "	
	200 man-hours @ $15/hr	$ 3,000
Material		
1 x 2-1/2 x 80 ft stl bar = 0.25 x 680 ft		170
3/8 x 3 stl bar		204
	Magnet assembly cost	$ 3,374

AUTHOR J. Gunn | DEPARTMENT Mechanical Engineering | LOCATION Berkeley

DATE December 2, 1974

NON MAGNETIC ABSORBER COSTS

Cast with wedged sides so as to fit into steel plates (90 plates)

11,332 # cast @ 80¢/lb $ 8,985

ENGINEERING DESIGN AND DRAFTING

160 hr @ $20/hr $ 3,200

SUPPORT (BASE) FOR MAGNET

Pour two concrete piers, 56 ft long $ 2,500

TOTAL	$240,173
Contingency 15%	36,026
GRAND TOTAL	$276,199

Inflation should be provided for at about 1% per month, for the appropriate time.

JG/DR:mp

APPENDIX 2 - INSTRUMENTATION COST ESTIMATE

Note: These cost estimates do not include institutional overhead costs. These have not been included because the method of calculation for overhead varies markedly from one institution to another making comparison difficult. Currently, 37% overhead is applied to materials and salary at LBL and 88% overhead is applied only to salary at Princeton. The estimates include shop labor charges for fabrication, assembly, and checkout wherever appropriate.

Calorimeter Counters (75 total)

Material	
Scintillator	on hand at LBL
Photomultipliers & bases	on hand at LBL
Light pipes, Al foil, etc.	$1425
Labor	$4135
TOTAL	$5560

Trigger Counters (64 total)

Material	
Scintillator	on hand at LBL
Photomultipliers & bases	on hand at LBL
Light pipes, Al foil , etc.	$ 512
Labor	$4557
TOTAL	$5069

Multiwire Proportional Chambers (20 total - 3 planes each)

Material (Al plate, G10, Wire, etc)	$22,521
Labor	
Electrical Shop	$ 7,276
Mechanical Shop	$ 7,741
Carpenter Shop	$ 565
TOTAL	$38,103

Drift Chambers (20 total - 1 plane each)	
Material (G10, wire, etc.)	$ 12,560
Labor (estimate)	20,000
TOTAL	$ 32,560
MWPC Electronics (4096 channels on hand; 8864 channels (+10% spares) to be constructed)	
Sense planes	
4096 channels	on hand at LBL
Additional 1952 channels + 10% spares @ 7.65	$ 16,426
Delay cable for above	on hand at Princeton (on loan to Fermilab Exp. 26)
Induced Planes	
6912 channels +10% spares @ 8.75	$ 66,528
TOTAL	$ 82,954
Drift Chamber Electronics	
320 channels @ $100	$ 32,000
Beam Telescope Counters and MWPC System	(partially on hand at Princeton) $ 2,000
Fast PDP-15 Camac Interface (estimate)	$ 5,000
Engineering and Drafting for Magnet Design	$ 3,200
GRAND TOTAL	$206,446

APPENDIX 3 - RESPONSIBILITIES AND PERSONNEL

I. Responsibilities for Design and Construction of the Spectrometer

A. Magnet

The cost of construction and installation of the magnet will be borne by the Fermilab. The engineering design, preparation of working drawings and supervision of fabrication and installation will be the responsibility of the experimenters. The design and drafting will be done at LBL, and the supervision of construction and installation will be performed by the Princeton and Fermilab contingents.

B. Instrumentation

The design and construction of the MWPC system, calorimeter, and trigger counters will be the responsibility of the LBL group. The drift chamber system, halo veto and beam telescope counters and small MWPC's will be the responsibility of the Princeton group. Interfacing the existing muon beam proportional chambers upstream of the muon lab (part of the muon scattering facility) to our system will be the responsibility of our Fermilab collaborator.

Standard fast-logic modules, photomultiplier power supplies, CAMAC crates, etc., will be supplied by PREP. For on-line use, a PDP-15 computer (48K core, 2 tapes) now at Princeton will probably be available. We are also considering the use of a standard BISON PDP-11 computer supplied by Fermilab.

II. RESPONSIBILITIES FOR OPERATION

The usual incidental supplies and expense (e.g., MWPC gas, travel, maintenance, etc.) will be the joint responsibility of the experimental groups. During installation, testing, and data collection the groups will maintain the following full-time equivalent manpower in residence at the Fermilab:

From LBL	3.5 FTE Ph.D. Physicits
	2.0 FTE Technicians
	$\geq$ 2.0 FTE Graduate Ph.D. Thesis Students
From Princeton	1.5 FTE Ph.D. Physicits
	0 or 1 FTE Graduate Ph.D. Thesis Student
From Fermilab	.5 FTE Ph.D. Physicists
TOTALS	5.5 FTE Ph.D. Physicists
	2.0 FTE Technicians
	2 - 3 Graduate Students

III. RESPONSIBILITIES FOR DATA ANALYSIS

Analysis of the data will be the joint responsibility of the experimenters. Preliminary tape compression will be performed on the Princeton PDP15 when it is not in on-line service. A large part of the event reconstruction will be done by the LBL 7600. Analysis of summary data will be performed at each institution.

IV. COMMITMENTS TO OTHER EXPERIMENTS BY PARTICIPANTS IN THIS PROPOSAL

LBL

A.R. Clark	Bevalac Exp. 209H (Complete CY75)
E.S. Groves	ISR (Letter of intent for experiment in FY77)
L.T. Kerth	Bevalac Exp. 209H (Complete CY75)
S.C. Loken	Fermilab Exp. 26 (Complete mid-year CY75)
M. Strovink	Fermilab Exp. 26 (Complete mid-year CY75)
W. Wenzel	ISR (Letter of intent for experiment in FY77)

PRINCETON

R. Cester	BNL Exp. 661 (CY75)
	Fermilab Exp. 302*
	BNL Exp. 646 (CY77)
F.C. Shoemaker	No other research commitments
M.S. Witherell	BNL Exp. 661 (CY75)
	Fermilab Exp. 302*
P. Surko	No other research commitments

FERMILAB

R.P. Johnson	Fermilab Exp. (Complete CY75)

*Fermilab E302 has first priority on the research activities of R. Cester and M.S. Witherell. If construction of the E302 $\bar{p}$ beam occurs on a schedule which results in an overlap between installation of E302 and operation of this experiment, the Princeton group intends to maintain its strength by bringing other scientific personnel into the experiment.

V. COMMUNICATION WITH THE FERMILAB

At present, the spokesman for the experiment is M. Strovink. During the construction phase of the experiment, the spokesman will be L.T. Kerth. During installation and operation of the experiment, communication with the laboratory will be the responsibility of one or more of the experimenters who are in residence at the Fermilab.

APPENDIX 4 - TRIGGER LOGIC AND BEAM REOUIREMENTS

A. General Considerations

Figures 1-3 indicate the calorimeter counters and hodoscopes which will be used for all trigger logic. We shall describe how the counter system can be used to study the various processes discussed in the proposal. Features which are common to all these conditions, the muon beam and associated muon halo, will be considered here.

1) Muon Beam:

The beam logic requires that the incident muon pass through the last bend in the muon beam (enclosure 104) without hitting the magnets. A beam hodoscope at 104 allows determination of muon angle. A fine grained hodoscope (10 x 10 counters) at the front of the spectrometer completes this angle measurement. In addition, requiring one and only one count in the hodoscope will eliminate all but 2% of the R.F. buckets containing two beam muons (see discussion of two muon trigger). To suppress further the background trigger rate from two muons in the same R.F. bucket, a third beam hodoscope at the downstream end of the spectrometer measures deflection perpendicular to the bend plane of the magnet. This is used to veto beam muons which are not scattered by more than multiple Coulomb scattering in the magnet. These two measures result in a suppression of 10^{-3} or better for two simultaneous beam muons.

2) Halo Veto:

A large counter array in front of the spectrometer (see Figure 1) is used to veto possible triggers from accidental beam halo coincidences. In order to construct a highly efficient counter with good time resolution we use the knowledge about the spatial distribution of halo muons gained from previous muon running. By using small counters close to the muon beam with larger ones outside (with less stringent requirements), we expect to obtain a halo suppression of 10^{-4}.

B. Two Muon Trigger

The trigger for M^o events uses calorimeter counters C1-C75 and trigger hodoscopes T1-T8. A trigger signifying a hadron interaction will use the fact that a typical hadron shower is spread through at least one entire module (5 iron slabs and counters) whereas an electromagnetic shower loses essentially all its energy in one slab (6 rl). A multi-muon final state requires two or more separate counts in a given bank of trigger hodoscopes. A coincidence from three sequential hodoscopes, separated by a total of 60 radiation lengths, is used to suppress trigger background from multiple showers. To suppress triggers from penetrating hadronic showers, the vertex location from the calorimeter counters is used to deaden hodoscopes immediately downstream of the vertex. On average, 3200 g/cm^2 of iron protect the hodoscope coincidence from remnants of the upstream shower. A Monte Carlo simulation of this trigger system yields a detection efficiency which varies from 45% at a M^o mass of 2 GeV/c^2 to 56% for M^o's of 10 GeV/c^2.

Background Triggers:

The most serious source of background triggers is associated with two beam muons in the same RF bucket. One of the muons interacts giving the required hadronic shower and the two muons are detected downstream. This rate is easily estimated.

Probability of two muons in the same RF bucket (at 10 MHz)	0.2
Probability of not vetoing two muon bucket (see previous discussion.)	$<10^{-3}$
Interaction probability (deep inelastic scattering with $\nu > 15$ GeV)	1.2×10^{-2}
Trigger Rate	2.4×10^{-6}

Triggers from the remnants of hadronic showers are eliminated by requiring a separation of seven modules (12 ft of iron) between the vertex and the last hodoscope in the coincidence. The rate can be estimated:

Probability of interaction with $\nu > 25$ GeV	6.5×10^{-3}
Probability of 12 ft penetration*	10^{-4}
Trigger Rate	6.5×10^{-7}

A third background trigger comes from multiple showers. The requirement that three hodoscopes in sequence detect more than one particle will eliminate this problem since the banks are separated by a total of 60 RL. For the case of multiple electromagnetic showers we get

Probability of interaction $\nu > 15$ GeV	1.2×10^{-2}
Probability of three independent electromagnetic showers	$(3 \times 10^{-2})^3$
Trigger Rate	3×10^{-7}

For the case of two hadron interactions, one of which penetrates four modules and triggers the hodoscopes the rate is lower.

Interaction Probability $\nu > 15$ GeV	1.2×10^{-2}
Probability of a hadron shower penetrating four modules	10^{-5}
Trigger Rate	1.2×10^{-7}

RF buckets which have a halo muon and a beam muon will be vetoed (see previous discussion). Any inefficiency in this veto will cause accidental triggers.

Probability of interaction $\nu > 15$ GeV	1.2×10^{-2}
Probability of halo in the same RF bucket	$< .2$
Veto inefficiency	10^{-4}
Trigger Rate	2.4×10^{-7}

* O. Fackler (private communication)

C. Deep Inelastic Muon Scattering Trigger

Real Rate

The trigger rate for real events from inelastic muon scattering is based on a Monte Carlo calculation with the following assumptions:

Beam: E_o = 225 GeV; size - 6" high x 8" wide; beam is incident on the face of the spectrometer centered horizontally and 6" below the median plane.

Cross Section: νW_2 is taken from a parameterization of the SLAC data.

Spectrometer: As described in Section II above.

Trigger: Scattered mu is required to pass through two successive trigger banks outside of the beam-veto region.

The beam muon and the scattered muon have been propagated through the iron by the simulation program, including the effects of single- and multiple-Coulomb scattering, μ-e scattering and muon bremsstrahlung.

Rate for real triggers 2.2×10^{-6}

Background Rates:

The most important backgrounds come from two step processes where the incident muon suffers a large energy loss and is deflected out of the spectrometer without triggering, and a scattered muon is faked by either an accidental halo muon or by long range "punch-through" from a hadronic shower.

We have made conservative estimates of these various trigger rates. Muon losses from μ-e scattering, bremsstrahlung, and low Q^2, high-ν inelastic scattering were studied with Monte Carlo programs. Data on punch-through was obtained from Fermilab experiment E-104*; an instantaneous beam rate of 10^7/sec and a halo veto inefficiency of 10^{-4} were assumed. The resulting rates are shown below:

---

* O. Fackler (private communication)

a) Beam loss rate from coulomb and μ-e scattering and muon bremmsstrahlung 5.5×10^{-4}

Probability of halo accidental 0.2

Halo veto inefficiency 10^{-4}

Total Rate 0.11×10^{-7}

b) Rate for low-Q^2 high ν inelastic scatter with scattered muon lost from beam veto; the scattered muon signature is completed by hadron punch through. This is calculated by folding together the depth-dependent muon loss rate and the probability of punch-through beyond that point. The minimum punch-through rate used was 2×10^{-3}.

Total Rate 0.4×10^{-6}

c) Same as b) except that the trigger is completed by a halo accidental.

Rate for loss of scattered muon from beam veto 1.1×10^{-4}

Probability of halo accidental 0.2

Halo veto inefficiency 10^{-4}

Total Rate 0.02×10^{-7}

Total rate - real + background 2.61×10^{-6}

D. Three Muon Trigger

Three-muon final states not associated with a hadron shower at the interaction vetex do not satisfy the multimuon-shower trigger described in (B) above. For this case a shower-independent trigger will be used, which requires at least three counts in each of three successive trigger hodoscopes. Background triggers from hadron showers [see (B)] are suppressed by requiring at least two of the banks to have exactly three counts. With this requirement, accidental counts from soft electromagnetic showers in the iron upstream of each counter will create a negligible inefficiency.

More serious trigger background is caused by muon tridents which have large (~1 μb/nucleus) production cross section. The most common tridents have small pair energy and opening angle. These are suppressed by requiring one of the three counts in each hodoscope to be separated from the beam area by ≈6" in the vertical

(nonbending) plane. The soft pair muons are bent out of the spectrometer active area before their vertical Coulomb scattering displacement exceeds ≈2". Fortunately, the mean vertical displacement at the exit from the active area varies only with the fourth root of the muon energy. The detailed muon-trident simulations which will set the limit on this background trigger rate are not yet complete.